9

THE ELECTRICAL CONDUCTIVITY OF LIVING TISSUE: A PARAMETER IN THE BIOELECTRICAL INVERSE PROBLEM

Maria J. Peters, Jeroen G. Stinstra, and Ibolya Leveles

Faculty of Applied Physics, Low Temperature Division, University of Twente

9.1 INTRODUCTION

Electrically active cells within the human body generate currents in the tissues surrounding these cells. These currents are called volume currents. The volume currents in turn give rise to potential differences between electrodes attached to the body. When these electrodes are attached to the torso, electrical potential differences generated by the heart are recorded. The recording of these electrical potential differences as a function of time is called an electrocardiogram (ECG). ECG measurements can be used to compute the generators within the heart. This is called the solution of the ECG inverse problem. This solution may be of interest for diagnostic purposes. For instance, it can be used to localize an extra conducting pathway between atria and ventricles. This pathway can then subsequently be removed by radio-frequent ablation through a catheter. When the active cells are situated within the brain and the electrodes are attached to the scalp, the recording of the potential difference measured between two electrodes as a function of time is called an electroencephalogram (EEG). The EEG inverse problem can, for example, be used to localize an epileptic focus as part of the presurgical evaluation. The frequencies involved in electrocardiograms and electroencephalograms are in the range of 1–1000Hz. Therefore, the Maxwell equations can be used in a quasi-static approximation, implicating that capacitive and inductive effects and wave phenomena are ignored as argued by Plonsey and Heppner (1967).

To solve the inverse problem a model is needed of the source and the surrounding tissues, *i.e.* the volume conductor. Customarily, the source is modeled by a current dipole or a current dipole layer and the volume conductor is described by a compartment model,

where all compartments are considered to be homogeneous. The head may have a scalp, a skull, a cerebrospinal fluid and a brain compartment. The torso compartment model may include the ventricular cavities, the lungs and the surrounding homogeneous medium. The shape may be a rough approximation of the real geometry, or the surfaces of the various compartments may have a realistic shape that is obtained from magnetic resonance images. An electrical conductivity is assigned to each compartment. If the inverse solution is used to localize the sources of the measured potentials, then only the ratio between the conductivities assigned to the various compartments is of importance. If the inverse solution is also used to estimate the strengths of the sources, then the absolute values of these conductivities are of importance.

In general, the conductivities of the various human tissues are among other things dependent on the blood content and temperature, they are a function of the frequency and strength of the applied current, they show an inter-individual variability, and they are inhomogeneous and anisotropic (Robillard and Poussart, 1977; Rosell *et al.*, 1988; Law, 1993). Moreover, the conductivity may be dependent on the health of the subject, for instance, edema will change the conductivity, so does the presence of scar tissue or tumors. The conductivity is called inhomogeneous when the conductivity differs from place to place. The conductivity is called anisotropic when the conductivity is different in different directions. For low current densities, the current density is linear with the applied electric field, in other words the law of Ohm is valid in this case. The averaged Ohmic conductivity that is assigned to a compartment is called the effective conductivity. The effective conductivity of an inhomogeneous tissue is the conductivity of a hypothetical homogeneous medium, which mimics the potential distribution that is found outside the inhomogeneous tissue. For instance, in case of EEG, the effective conductivities assigned to the various tissues in the head have to give approximately the same potential distribution at the scalp as the real inhomogeneous tissues. The problem addressed in the present chapter is: Which value should be assigned to a certain compartment?

9.1.1 SCOPE OF THIS CHAPTER

In order to estimate the effective conductivity of a certain tissue, two approaches are possible. First, the conductivity of a tissue can be measured *in vitro* or *in vivo* by applying a potential difference by means of a set electrodes and measuring the resulting current. A second approach is applying knowledge of the chemical composition and biological morphology of the tissue in order to compute the effective conductivity. As measured values of the effective conductivities of tissue reported in the literature vary widely, the second approach may be of help to restrict the uncertainties in the conductivities involved in the volume conduction problem. In section 9.1.2, the concept that the conductivity is not a straightforward property of the material is discussed. The effective conductivity from an experimental point of view will be discussed in section 9.1.3.

In section 9.2 the tissue is modeled as a suspension of cells in an aqueous surrounding. If only one type of cells is present and the suspension is a dilute one, the effective conductivity is expressed by Maxwell's mixture equation. This equation will be discussed in section 9.2.3. If more than one type of cell is present and the cells are densely packed or clustered, the effective conductivity is expressed by Archie's law. This will be the subject of section 9.2.4. The applicability of Maxwell's mixture equation and Archie's law will be illustrated for various tissues, such as blood, fat, liver, and skeletal muscles.

In section 9.3, it is taken into account that most tissues have a layered structure, each layer having a different conductivity. The effective conductivity of an entire compartment will be discussed in section 9.4. The conductivity of a composite medium, like human tissue, cannot have any value but will be within certain limits. section 9.5 of this chapter is dedicated to these limits.

9.1.2 AMBIGUITY OF THE EFFECTIVE CONDUCTIVITY

Electrical currents in the human body are due to the movements of ions. As a result of an electric force acting on an ion that is dissolved in fluid, the ion will develop a mean drift velocity between collisions. Despite the fact that the average spacing between cells may be no more than 20 nm, the mean free path of an ion in the extracellular space is only about 0.01 nm. This represents the distance between collisions with other molecules. Almost all these collisions take place with water. An ion rarely encounters a cell membrane and behaves most of the time as though it were in a continuum. The drift velocity in Ohmic conductors is directly proportional to the electric field. The current density reads:

$$\vec{j} = \sigma \vec{E} \tag{9.1}$$

where σ is the conductivity and E the electric field.

The electrical conductivity cannot be determined unambiguously, because it depends on the direction of the currents, the extent of the current source, and the positions of the measuring electrodes. This is illustrated in Fig. 9.1 where two different situations are compared. In the first situation, a uniform current is applied between two parallel flat electrodes. In the second situation the current is generated by a point source. The expressions for the conductivity are different for the two situations showing that the effective conductivity is not merely dependent on the material, but also on the configuration given by the orientation and location of the source and the measurement points.

If a medium is piece-wise homogeneous and isotropic then the proper boundary conditions are that the normal component of the current density is continuous and the normal

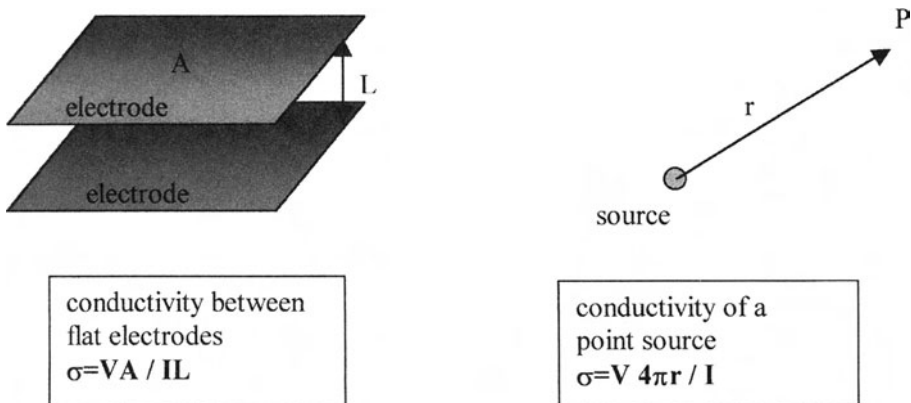| conductivity between flat electrodes $\sigma = VA / IL$ | conductivity of a point source $\sigma = V\,4\pi r / I$ |

FIGURE 9.1. This figure illustrates that the conductivity measured in a homogeneous medium of infinite extent depends on the electrodes used.

component of the dielectric displacement makes a step that is equal to the surface charge density. Hence, all interfaces (including the outerfaces of the cells) will have a continuous distribution of surface charge representing genuine accumulations of charge. If the material is non-uniform or if the conductivity is anisotropic, we get accumulations of charge within the material as well as on the interfaces.

The microscopic electrical conductivity is the conductivity that characterizes a part of tissue that is comparable in size with the dimensions of the cells. The macroscopic effective conductivity characterizes a part of the tissue that is large compared to the dimensions of the cells. Several levels of inhomogeneities can be distinguished. We will restrict ourselves to three levels of inhomogeneities, the microscopic level with typical dimensions of microns, the millimeter level and the macroscopic level, e.g. compartments with dimensions of several centimeters. This is illustrated in Fig. 9.2. In the microscopic point of view, forms and dimensions of cells and the interstitial fluid are taken into account. Near a cell, the electrical field may change in direction or amplitude due to the charge density on the surface and the presence of counterions near the surface. For macroscopic purposes one has to consider the field averaged over regions large enough to contain many thousands of cells or fibers so that microscopic fluctuations are smoothed over, the 'graininess' of the material is blurred by distance. At a millimeter level, the layered structure or columnar structure of an organ is taken into account. For instance, the skin is composed of three layers, namely the epidermis (the outer non-sensitive and non-vascular layer of the skin that overlies the dermis), the dermis and subcutis. The epidermis is composed of stratum corneum, stratum lucidum, stratum granulosum and stratum germinativum. These layers differ in composition and morphology and consequently in conductivity. The conductivity of the various layers is averaged and the material acts as a continuum, the averaged conductivity being the effective conductivity.

9.1.3 MEASURING THE EFFECTIVE CONDUCTIVITY

The uncertainty in measured conductivity values is high, because the measurements are very complicated. The reasons why they are so complicated will be shortly discussed in this section. Usually, the Ohmic low-frequency conductivity of a piece of tissue is determined from the current-voltage relation using a two- or four points method. The currents used for the measurements have to be low (about 1mA) in order not to trigger an activation of cells. The field near one cell is very much influenced by the presence of the cell. In order to have an effective conductivity thousands of cells have to be present within the piece of tissue measured. Therefore the effective conductivity has to be measured with electrodes with dimensions of millimeters, these electrodes have to be millimeters apart. The sources in the brain and heart of EEG and ECG are due to at least 10^5 cells that are active in synchrony else the EEG or ECG would not be measurable. Consequently, the condition that the source has dimensions of millimeters is met if brain or heart activity is used for conductivity measurements.

If the measurements are carried out *in vitro* (*i.e.* outside the body), the accuracy may be low because tissue properties change after death. The conductivity will initially drop after circulatory arrest due to emptying blood vessels and drainage of fluids. For instance, it was found that the conductivity of frog muscle at 10Hz decreased a factor two after 2.5 hours of death and that of chicken muscle decreased 70 percent in the first 60 minutes (Zheng *et al.*,
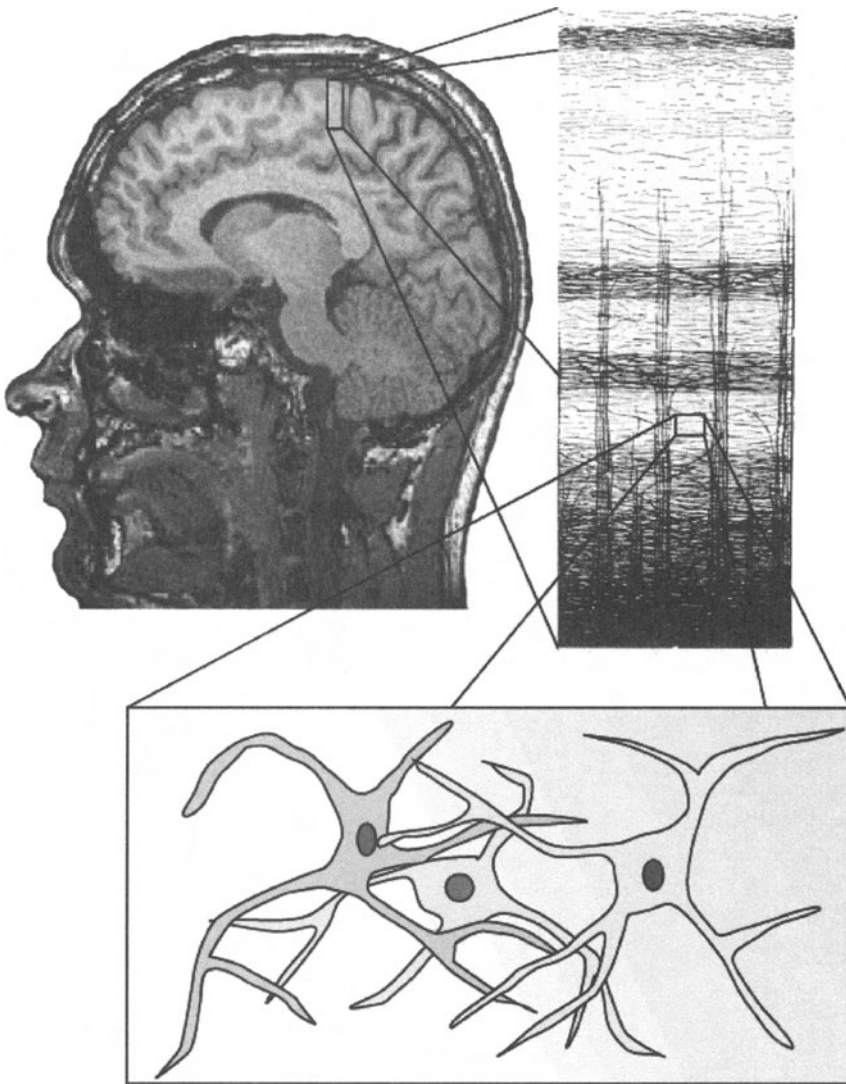
FIGURE 9.2. Illustration of the three levels of inhomogeneities discussed in this chapter. at the left) the head that is usually modeled by three compartments; in the middle) the layered gray matter; at the right) a suspension of cells.

1984). However, the conductivity of dog muscle increased immediately after death (Zheng *et al.*, 1984). This may be caused by a change in the osmotic pressure causing some cells to swell and burst. Gielen (1983) measured *in vivo* the low-frequency conductivity of the muscles of a rabbit that were prepared free, the blood supply was unimpaired. He found after finishing his experiments that the outermost muscle layer was damaged. The cross sections of the fibers were much larger and rounder than normal. This damage was related to an increase in conductivity. This phenomenon was blamed to osmotic processes. The increase

will grow in time (Schwan, 1985), because cell membranes after death allow currents to pass more easily. In other words, all *in vitro* conductivity measurements should be completed within a very limited time.

If the measurements are carried out *in vivo*, commonly animal tissue instead of human tissue is used. However, it is not clear whether the animal tissue has the same electrical properties as human tissue although sometimes they seem to be comparable. Moreover, the *in vivo* measurements depend on the surrounding tissues. When electrodes are implanted in living tissue, the currents applied by these electrodes will not be confined to the tissue that is between the electrodes, but will spread out through all surrounding tissues. Hence, it is difficult to estimate which part of the current will flow through the tissue of interest. Some investigators try to avoid this problem by measuring the conductivity with two electrodes spaced closely together. However, this raises the question whether on such a scale the inhomogeneities in the structure of the tissue do not disable the measurement of an effective macroscopic conductivity because the electric field within the tissue near cells has a complicated pattern. If one happens to be near a cell, the field may be small or point in a totally different direction. Another problem experienced is a relatively large extra capacity between electrode and tissue at low frequencies. Moreover, the electrode-electrolyte interface can produce large errors that depend on the pressure between electrode and organ tissue.

Thence, it is not surprising that the measured low-frequency conductivities reported in the literature vary over a wide range. As example some values found for the low-frequency conductivity of skeletal muscle tissue at 37°C are given in table 9.1. No attempt to give a complete overview has been made. The conductivity in muscle tissue is anisotropic, the conductivity along the fibers σ_h is higher than the conductivity perpendicular to the fibers σ_l. Five degrees misalignment from true parallel or perpendicular orientation during the measurement would result in an 18 percent overestimate of σ_l and a 0.4 underestimate of σ_h (Epstein and Forster, 1983). Consequently, misalignment errors will be smallest in σ_h and the anisotropy factor will be easily underestimated. Out of theoretical studies, there might develop insight into the nature of volume conduction that would permit a proper choice from the values that are reported.

TABLE 9.1. Some values found in the literature of the conductivity of skeletal muscle at 37°C in the frequency range of 0–1000 Hz

species	σ_h(S/m)	σ_l(S/m)	anisotropy factor σ_h/σ_l	reference
cow	0.41	0.15	2.7	Burger and van Dongen (1961)
rabbit	0.8	0.06	13	,,
dog	0.67	0.04	17	Rush *et al.* (1963)
dog	0.43	0.21	2.0	Burger and van Milaan (1943)
frog(21°C)	0.09	0.05	1.8	Hart *et al.* (1999)
dog	0.70	0.06	11	Zheng *et al.* (1984)
rabbit	0.75	0.04	17	,,
monkey	0.81	0.06	13	,,
dog	0.52	0.08	6.5	Epstein and Foster (1983)
rabbit	0.5	0.08	6.3	Gielen *et al.* (1984)
rat	0.5	0.07	6.1	McCrae and Esrick (1993)

TABLE 9.2. Examples of the temperature dependence of tissues

material	conductivity (S/m)	temperature (°C)
bile (cow-pig)	1.66	37
	1.28	20
amniotic fluid (sheep)	1.54	25
	2.04	37.5
Urine (cow-pig)	3.33	37
	2.56	20
skeletal muscle (rat)		
parallel	0.42	36.7
	0.66	44.5 (after 30 minutes)
perpendicular	0.08	36.6
	0.20	44.5 (after 30 minutes)

9.1.4 TEMPERATURE DEPENDENCE

The electrical conduction in living tissue depends on the temperature. Mc Rae and Esrick (1993) heated freshly excised rat skeletal muscle from 39.5 to 50°C. Above 44°C healthy tissue will be damaged irreversibly. Initially, a rapid increase of the low-frequency conductivity (with about a factor two) was observed followed by a much slower increase during which the low-frequency conductivity gradually approached the high-frequency values. The initial rapid change was associated with microscopically observed fiber rounding and shrinkage in the radial direction and increasing edema. The subsequent slow change was associated with disintegration of the tissue. After the cell membranes are destroyed, the conductivity is no longer frequency dependent and the low-frequency conductivity has the same value previously measured at high frequencies. The temperature dependency of the conductivity of tissue is also caused by the temperature-dependent regulation of the vessel diameter (vasodilatation). In other words, the blood supply is temperature dependent. The temperature dependence of the conductivity is illustrated in Fig. 9.3 and table 9.2.

9.1.5 FREQUENCY DEPENDENCE

The low-frequency conductivity of most tissues like heart muscle, skin, liver, lung, fat, and uterus is not strongly dependent on frequency, although measurements show that the conductivity increases with frequency, also at low frequencies. Commonly, this phenomenon is not taken into account and the conductivity is presumed to be frequency independent for frequencies lower than 1000Hz (e.g., Schwan and Foster, 1980). Nevertheless, the conductivity does increase with the frequency regardless the kind of tissue. Nicholson (1965) measured the conductivity of cerebral white matter of a cat. He found an enhancement of the conductivity in the direction normal to the fibers from 0.11S/m to 0.13S/m, when the frequency changed from 20 to 200Hz. No enhancement was found for the conductivity parallel to the fibers. Comparison between the experimental data presented by Gabriel et al. (1996[a]), and corresponding data previously reported in the literature show good agreement (Stuchly and Stuchly, 1980). The conductivity of the gray matter as measured by Gabriel et al. (1996[b]) in the frequency range from 10Hz to 20GHz is given in Fig. 9.4.
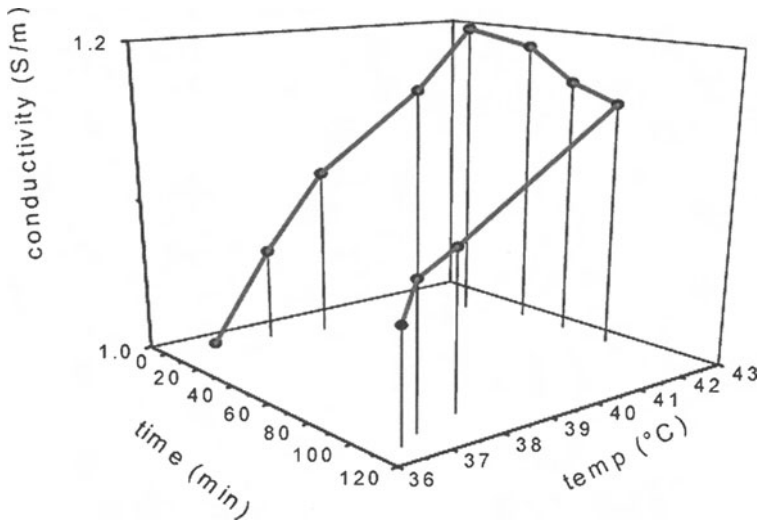
FIGURE 9.3. Variation of the conductivity with the temperature and time for skeletal muscle, based om measurements reported by Gersing (1998).
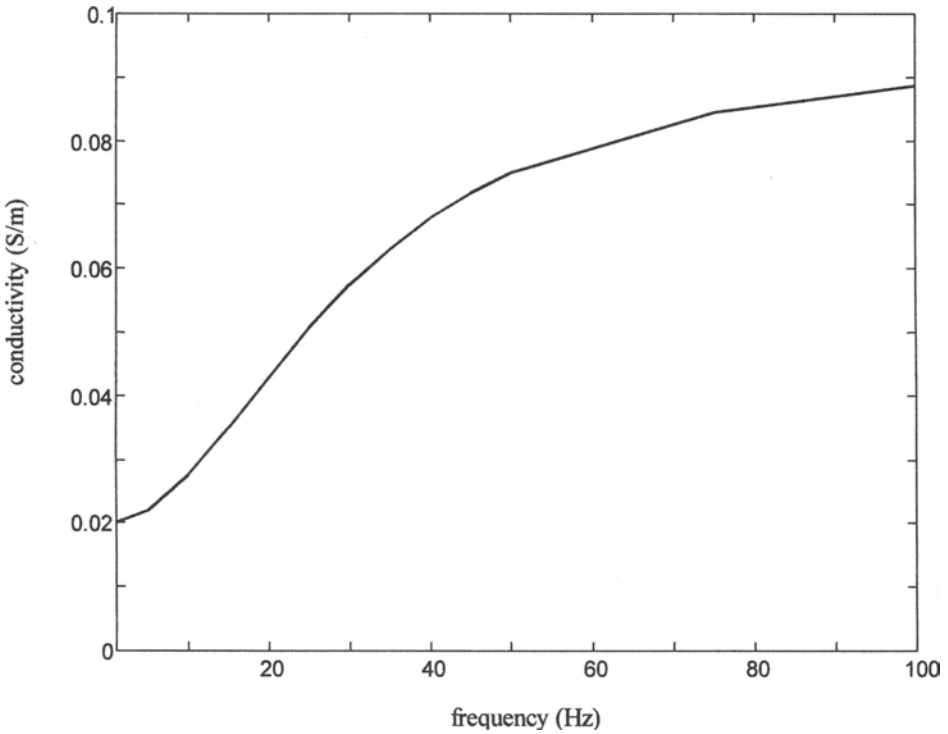

FIGURE 9.4. The frequency-dependent conductivity of gray matter based on the parameters given by Gabriel et al. (1996[b]).

9.1.5.1 Impact of the frequency dependence on the EEG

The frequency dependence of the conductivity may influence the EEG. In order to estimate the impact on EEG, the effects of a frequency-dependent conductivity were simulated. The volume conductor model consisted of three concentric spheres representing the brain, skull and scalp, with radii of 87, 92 and 100mm. This model is often used to describe the head as a volume conductor. The source was modeled as a current dipole. Simulations were carried out for three current dipoles, *i.e.* a central dipole, and a radial and a tangential dipole at a radius of 80mm. As observation point, a point at the surface was taken where the potential, found for the lowest frequency, was maximal. The transfer function was calculated. The transfer function is the relationship between the strength of the current dipole and the potential in a point at the outermost surface as a function of the frequency. To enable a comparison between the different cases, all transfer functions were normalized. If there is no frequency dependence, the transfer function would have the value one for all frequencies.

Two cases were studied. First, the gray matter conductivity was taken from Fig. 9.4 in which the conductivity increases by a factor four; the scalp conductivity was 0.33S/m and that of the skull 0.0042S/m. Second, the conductivity of all compartments increased 20% in the interval from 1Hz to 100Hz. At 1Hz the conductivity of the brain and scalp was 0.33S/m and that of the skull 0.0042S/m. The results of these simulations are given in Fig. 9.5. As shown the volume conductor acts as a low-pass filter. The potential may drop by approximately a factor two when the frequency is increased from 1 to 100Hz. The transfer function depends on the depth of the source.

9.2 MODELS OF HUMAN TISSUE

Tissues are composed of cells. The interstitial space between the cells contains fluid. So, the effective conductivity of a tissue depends on the conductivity of the cells, the volume fraction occupied by the cells, and the conductivity of the extracellular medium.

9.2.1 COMPOSITES OF HUMAN TISSUE

This section starts with a brief description of tissue at a cellular level. Next, the conductivity of a cell and that of the extracellular fluid will be discussed.

9.2.1.1 Cells

All human cells stem from the round-shaped fertilized egg cell. There is no typical cell shape. Cells come in all shapes: cubes (cells lining sweat ducts), spheres (white blood cells of the immune system), Bismarck doughnuts (red blood cells), columnar cells, balloon-like cells (cells lining the urinary bladder), needle shaped ellipsoids or rods (skeletal muscle cells) and pancakes (cells on the surface of the skin) as illustrated in Fig. 9.6.

Cells vary also considerably in size, and function. For instance, the diameter of a red blood cell is 7.5μm, the diameter of a human egg cell is 140μm, a smooth muscle cell has a length of 20 to 500μm, while a skeletal muscle cell may have a length of 30cm. All cells
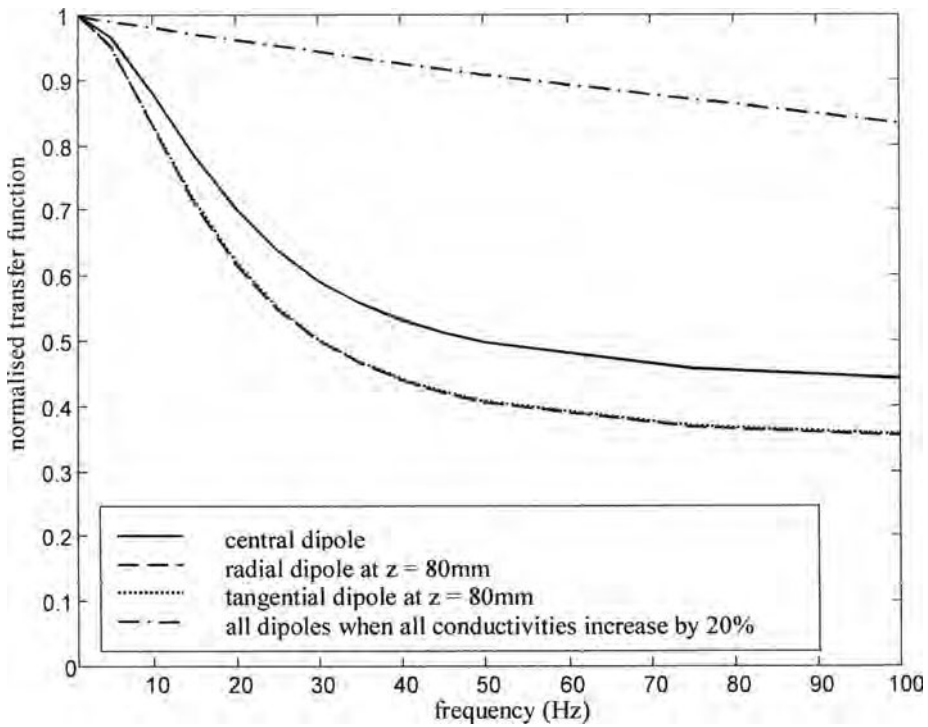
FIGURE 9.5. Transfer functions for EEG for three dipoles using a three-sphere model of the head. Two cases of frequency-dependent behaviour are considered. In the first case the conductivity of the brain compartment is chosen according to Fig. 9.4. In the second case the conductivity of all three compartments increases linearly.
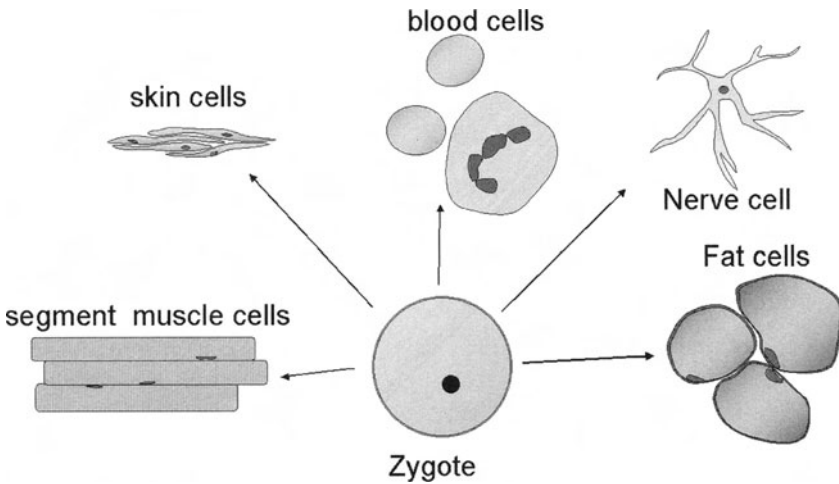

FIGURE 9.6. Cells vary considerably in shape.

TABLE 9.3. Values of a cell as found in the literature (adapted from Kotnik *et al.*, 1997)

cell values	lower limit	higher limit
extracellular medium conductivity σ_e	$5.0 \times 10^{-4}\,\text{Sm}^{-1}$	$2.0\,\text{Sm}^{-1}$
membrane conductivity σ_m	$1.0 \times 10^{-8}\,\text{Sm}^{-1}$	$1.2 \times 10^{-6}\,\text{Sm}^{-1}$
cytoplasmic conductivity σ_i	$2.0 \times 10^{-2}\,\text{Sm}^{-1}$	$1.0\,\text{Sm}^{-1}$
cell radius R	$1\,\mu\text{m}$	$100\,\mu\text{m}$
Average membrane thickness: t = 5 nm		

are surrounded by a membrane 5 to 10nm thick, visible only with the electron microscope. The electrical properties of the cell components are different. The highest and lowest values reported in the literature for the electrical properties of biological cells are given in table 9.3.

The intracellular fluid accounts for about 70 percent of the inner cell volume. The membranes maintain the integrity of the cell, breaking down after death. Membranes are highly selective permeability barriers and consist mainly of lipids and proteins. Lipid bilayer membranes have a very low permeability for ions and most polar molecules. An exception is water that easily crosses such membranes, and creates a balance in the whole organism. An ion such as Na^+ crosses membranes very slowly because the removal of its shell of water molecules is highly unfavorable energetically. Membranes contain specific channels and pumps that regulate the molecular and ionic composition of the intercellular compartment. A nerve impulse, or action potential is mediated by transient changes in Na^+ and K^+ permeability. An action potential is generated when the membrane potential is depolarized beyond a critical threshold value. When the transmembrane potential is not exceeding the threshold value, the relationship between the potential and the current is approximately linear, so it obeys Ohm's law. For low frequencies, this is the case when the current density is smaller than $0.5\,\mu\text{A/cm}^2$.

9.2.1.2 Volume fraction occupied by cells

One can analyse blood and determine the hematocrit content (the volume fraction occupied by the red blood cells) by measuring the electrical conductivity of blood. The electrical conductivity is a function of the hematocrit. This function is given in Fig. 9.7.

9.2.1.3 The extracellular fluid

Mammals have a water content of 65 to 70 percent. In the early fetal period of humans, approximately 95 percent of the fetus is water. The proportion of total body weight that is water decreases throughout the fetal period to reach 75 percent at term. The water content of various tissues of adults is given in table 9.4. Biological tissues are inhomogeneous materials with discrete domains: the extracellular and the intracellular space. Although the cells are of microscopic size, still they are much larger than the ions in the extracellular space so that the extracellular fluid can be considered as a continuum. The extracellular and intracellular fluids are electrically neutral, however, the ion concentrations are quite different in each. Thus, the electrical properties of the intracellular fluid and the extracellular fluid are different.

TABLE 9.4. Water content of various organs (Pehtig and Kell, 1987; Foster and Schwan, 1986)

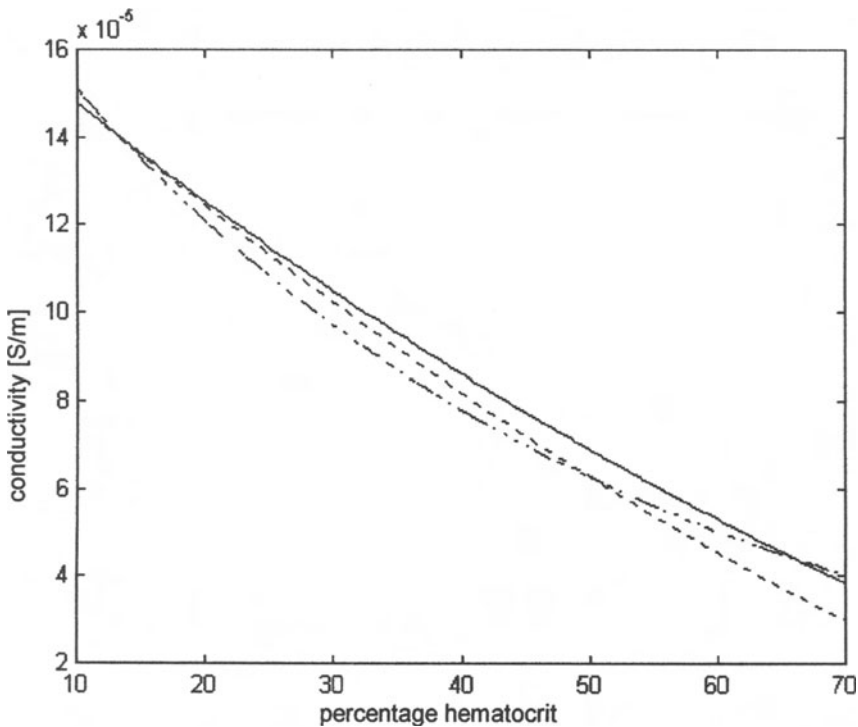| tissue type	volume fraction of water
gray matter (brain)	0.84
white matter (brain)	0.74
skeletal muscle	0.795
Fat	0.09
Liver	0.795
Spleen	0.795

FIGURE 9.7. The conductivity of blood as a function of the percentage of red blood cells (*i.e.* the hematocrit). The dashed line is the measured curve, the solid line is calculated using Maxwell's mixture equation, the line with points and dashes is calculated using Archie's law.

9.2.2 *CONDUCTIVITIES OF COMPOSITES OF HUMAN TISSUE*

A composite cell includes a nucleus, cytoplasm, and a cell membrane. The nucleus is enclosed by a thin cell membrane. The cytoplasm is a mass of fluid that surrounds the nucleus and is encircled by the plasma membrane. Within the cytoplasm are specialized structures called cytoplasmic organelles. In other words, the structure of a cell is such that the conductivity cannot be expected to be homogeneous. The effective conductivity is the
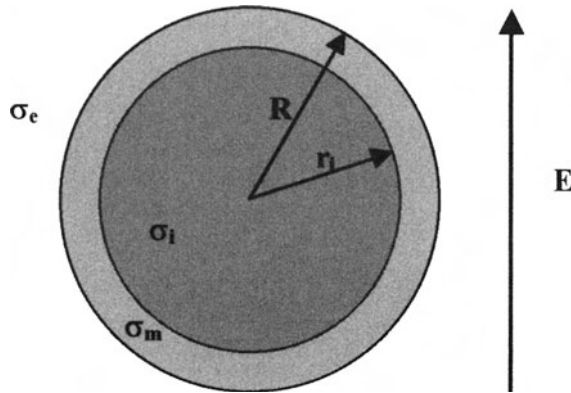
FIGURE 9.8. Model used to calculate the effective conductivity of a spherical cell.

conductivity ascribed to an entire cell. In the next section this effective conductivity is estimated using a simple model for the cell.

9.2.2.1 Effective conductivity of a spherical cell

The effective conductivity of a cell at low frequencies and for low current densities will be estimated for a spherical model of a cell. In the model, a sphere of radius r_i and conductivity σ_i is surrounded by a thin concentric shell of thickness t and conductivity σ_m representing the membrane. The cell is suspended in a medium with conductivity σ_e. The model is depicted in Fig. 9.8. Typically, t is 5nm for a cell and its radius $R = r_i + t$ is 10μm, thence $t \ll R$.

The law of conservation of charge in quasistatic approximation reads:

$$\vec{\nabla} \cdot \vec{j} = 0 \tag{9.2}$$

Inserting $\vec{j} = \sigma \vec{E}$ and $\vec{E} = -\vec{\nabla} V$ yields for a homogeneous region where σ is constant Laplace's equation

$$\nabla^2 V = 0 \tag{9.3}$$

We assume that a homogeneous electric field E is applied along the z-axis. The electrical potential outside the two-layered particle can be calculated by solving Laplace's equation with the proper boundary conditions. The boundary conditions are that the potential and the normal component of the current density are continuous across the boundary. On the other hand we can calculate the potential outside a homogeneous sphere of conductivity σ_{eff} suspended in a medium of conductivity σ_e. The effective conductivity of the cell is the conductivity of a uniform sphere that gives the same electrical potential outside the cell as the two-layered one. Equating the two solutions for the potential and neglecting the higher order terms of t/R in both the denominator and numerator as $t \ll R$, yields
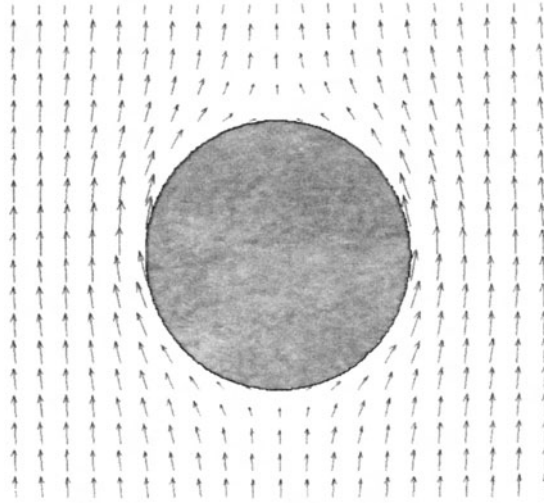
FIGURE 9.9. The current density around a spherical cell. The applied field was initially uniform. The intracellular current density is too small to be depicted.

(Takashima, 1989)

$$\sigma_{\text{eff}} = \sigma_{\text{m}} \frac{\sigma_i - 2t(\sigma_i - \sigma_{\text{m}})/R}{\sigma_{\text{m}} + t(\sigma_i - \sigma_{\text{m}})/R} \tag{9.4}$$

Inserting the values given in table 9.3 shows that cells can be described as non-conducting particles because the effective conductivity of a cell is about 10^{-5} times that of the surrounding fluid. In good approximation, at low frequencies the currents flow around the cells rather than through them as shown in Fig. 9.9. Thence, at low frequencies, the conductivity is dominated by the conductivity of the extracellular space.

9.2.2.2 Effective conductivity of a cylindrical cell

Similar calculations can be carried out to deter mine the effective conductivity of a cylindrical cell. We assume that a current is applied perpendicular to the axis. The effective conductivity reads

$$\sigma_{\text{eff,perp.}} = \sigma_{\text{m}} \frac{\sigma_i - t(\sigma_i - \sigma_{\text{m}})/R}{\sigma_{\text{m}} + t(\sigma_i - \sigma_{\text{m}})/R} \tag{9.5}$$

leading to the conclusion that in this case the cylindrical cell like the spherical one can be considered as a non-conducting particle.

However, if the field is applied parallel to the axis it is a different situation. The cell has a resistance for a current parallel with the axis. The resistance of an element of material

of length L and cross section A is

$$R = L/(\sigma A) \tag{9.6}$$

The cylindrical shell of thickness t, that represents the membrane, is connected in parallel with the inner cylinder of radius $(r - t)$. The part of the membrane at the top and that at the bottom of the cylinder are connected in series with the intracellular fluid of the cell. So the resistance reads

$$\frac{1}{R_{eff}} = \frac{\sigma_{eff}\pi r^2}{L} = \frac{\pi (r - t)^2}{\dfrac{L - 2t}{\sigma_i} + \dfrac{2t}{\sigma_m}} + \frac{\sigma_m 2\pi rt}{L} \tag{9.7}$$

where the effective conductivity is defined as the conductivity of an element of homogeneous material with the same dimensions, that has the same resistance as the inhomogeneous element. In good approximation expression (9.7) leads to the expression

$$\sigma_{eff} = \frac{\sigma_i \sigma_m L}{L\sigma_m + 2t\sigma_i} \tag{9.8}$$

Expression (9.8) is only true when the cells are intact, *i.e.* the membranes at the bottom and top of the cylinder are not damaged.

9.2.2.3 Conductivity of extracellular fluid

Since the intracellular space is not playing a role, as the effective conductivity of a cell is in general zero for low frequencies, the intracellular fluid is not considered here further. Materials with the highest conductivity are fluids with a low concentration of cells like urine, amniotic fluid, cerebrospinal fluid and plasma, which will be discussed below.

Using the ionic concentrations of the different cations and anions in the extracellular fluid, the conductivity can be approached by

$$\sigma = \sum_i \lambda_i c_i \tag{9.9}$$

where λ_i are the ionic conductivities at 37°C and c_i are the molar concentrations of the different ions. In table 9.5 the ionic conductivities of various ions at a temperature of 37°C are given as well as the ionic concentrations in the interstitial fluid, the cerebrospinal fluid and the blood plasma. Using these values, the conductivity of these fluids can be estimated. In table 9.6 the computed values are compared with the values cited in literature. From these values it becomes apparent that the computed values are about 15 to 25 percent higher than the measured values. This overestimation may be explained by the presence of proteins in the actual solution and the presence of counterions surrounding its cells.

The extracellular concentration of ions such as K^+ undergoes frequent small fluctuations, particularly after meals or bouts of exercise. An exception is the brain; if the brain

TABLE 9.5. The ionic concentration mmol/l of different fluids encountered in the body and the specific conductivity of each ion in a dilute solution at 37°C. The values were obtained from Aseyev (1998). *These values were only available for 25°C and have been corrected by 2 percent/°C

Ion	blood plasma	interstitial fluid	cerebrospinal fluid	$\lambda_i 10^{-4} Sm^2/mol$
Na^+	142	145	153	63.9
K^+	4	4	2	95.7
Mg^{2+}	2	1	3	142.4
Ca^{2+}	5	4	3	154.9
Cl^-	102	116	123	95.4
HCO_3^-	26	29		55*
PO_4^{3-}	2	2		296*
protein	17.0	0.0		
Other	6.0	6.7		

TABLE 9.6. Calculated and measured values of the conductivity of body fluids at 37°C. The measured values are taken from literature: [a]Geddes and Baker (1967), [b]Schwan and Takashima (1993), [c]Baumann et al. (1997)

conductivity of body fluids (at 37°C in S/m)	blood plasma	interstitial fluid	cerebrospinal fluid
computed	2.08	2.22	2.12
measured	1.58[a]	2.0[b]	1.79[c]

were exposed to such fluctuations the result might be uncontrolled nervous activity, because K^+ ions influence the threshold for the firing of nerve cells. The conductivity of electrolytes is dependent on the temperature. The conductivity of the amniotic fluid was measured by De Luca et al. (1996) at a temperature of 20°C. The mayor contributors to the conductivity are the Na^+ and Cl^- ions. The ionic conductivity of the former increases by 2.1 percent per °C and that of the latter by 1.9 percent per °C. An overall increase of $17 \times 2 = 34$ percent for the amniotic fluid heated from 20 to 37°C is thus expected. The same rate of increase was also obtained by Baumann et al. (1997), who measured the conductivity of cerebrospinal fluid at 25 and 37°C.

9.2.3 MAXWELL'S MIXTURE EQUATION

Spherical particles suspended in a solvent are considered to be a relevant model of biological tissues. Maxwell (1891) derived an equation for the effective conductivity of dilute suspensions in aqueous media of spherical particles (that do not have a permanent electric moment). The derivation of this equation is given in short below. Next, Maxwell's equation is extended for ellipsoidal particles, as many biological cells are better described by ellipsoids instead of spheres. The applicability of Maxwell's equation will be illustrated for blood.
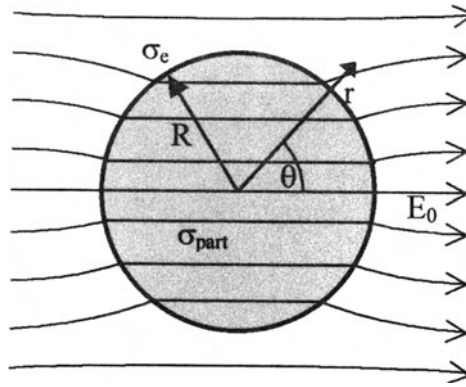
FIGURE 9.10. A spherical particle of conductivity σ_{part} surrounded by a solvent with conductivity σ_e placed in an original uniform field E.

9.2.3.1 A dilute solution of spheres

First, let us consider a spherical particle of radius R and conductivity σ_{part} embedded in a homogeneous solvent with conductivity σ_e when a uniform electric field E_0 is applied. An expression for the potential outside the sphere is found by solving the Laplace equation with the proper boundary conditions using spherical co-ordinates. The origin of the co-ordinates (r, θ, φ) is at the center of the sphere. This yields for the potential V outside the sphere of radius R:

$$V(r, \theta) = -\left(1 + \frac{\sigma_e - \sigma_{part}}{2\sigma_e + \sigma_{part}} \frac{R^3}{r^3}\right) E_0 r \cos\theta \qquad (9.10)$$

Within the sphere, the field is parallel and uniform. Outside the sphere, the field is the original field plus the field of a dipole at the center of the sphere (see Fig. 9.10).

Second, the suspension is modeled by N small spherical particles of radius R and conductivity σ_{part} that are surrounded by a large spherical boundary of radius R' as depicted in Fig. 9.11. Two assumptions are made. First, the volume fraction occupied by the cells is assumed to be low, the average distance between them being larger than their dimensions and as a consequence the spheres do not influence each other although they act as dipoles. The potential is the sum of the potential due to N small homogeneously distributed particles, yielding:

$$V(r, \theta) = -\left(1 + N\frac{\sigma_e - \sigma_{part}}{2\sigma_e + \sigma_{part}} \frac{R^3}{r^3}\right) E_0 r \cos\theta. \qquad (9.11)$$

Instead of the microscopic point of view, we can look at the sphere from a macroscopic point of view. We have a spherical shaped medium consisting of an aqueous solution of spherical particles. The effective conductivity of this sphere is per definition the conductivity that gives a potential outside of the sphere that is expressed by (9.10). Hence, the potential at
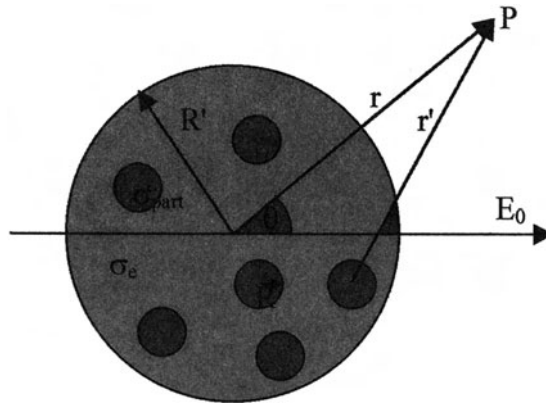
FIGURE 9.11. The model used for the derivation of the Maxwell mixture equation.

a distance r > R' from the center of the sphere describing the solution reads:

$$V(r, \theta) = -\left(1 + \frac{\sigma_e - \sigma_{eff}}{2\sigma_e + \sigma_{eff}} \frac{R'^3}{r^3}\right) E_0 r \cos \theta \qquad (9.12)$$

where σ_{eff} is the effective conductivity of the large sphere containing N particles.

Formulas (9.11) and (9.12) are equivalent expressions for the potential outside the sphere with radius R'. Noting that $NR^3/R'^3 = p$ is the volume fraction occupied by the particles that are suspended in the large spherical boundary we obtain by equating expressions (9.11) and (9.12) the so-called Maxwell's mixture equation:

$$\frac{\sigma_e - \sigma_{eff}}{2\sigma_e + \sigma_{eff}} = p\frac{\sigma_e - \sigma_{part}}{2\sigma_e + \sigma_{part}} \qquad (9.13)$$

As argued before at low frequencies and low current densities, the currents will in general be only in the extracellular space, in that case one can insert $\sigma_{part} = 0$.

A spherical model is a good approximation for many colloidal particles, including biological cells. However, biological cells often have a complex geometry. Many cells are better described by ellipsoids; a, b and c are the semi-axes of the ellipsoid. Maxwell's mixture equation has been derived for ellipsoidal particles that are orientated in parallel by Sillars (1937). When p is very low and the field is applied along the a-axis, it reads:

$$\sigma_{eff} = \sigma_e \left[1 + \frac{p(\sigma_{part} - \sigma_e)}{\sigma_e + (\sigma_{part} - \sigma_e)L_a}\right] \qquad (9.14)$$

where L_a is the depolarization factor of the ellipsoid in the direction of the a-axis, (Boyle, 1985).

$$L_a = \frac{abc}{2} \int_0^\infty \frac{ds}{(a^2 + s)\sqrt{(a^2 + s)(b^2 + s)(c^2 + s)}}; \qquad L_a + L_b + L_c = 1 \quad (9.15)$$
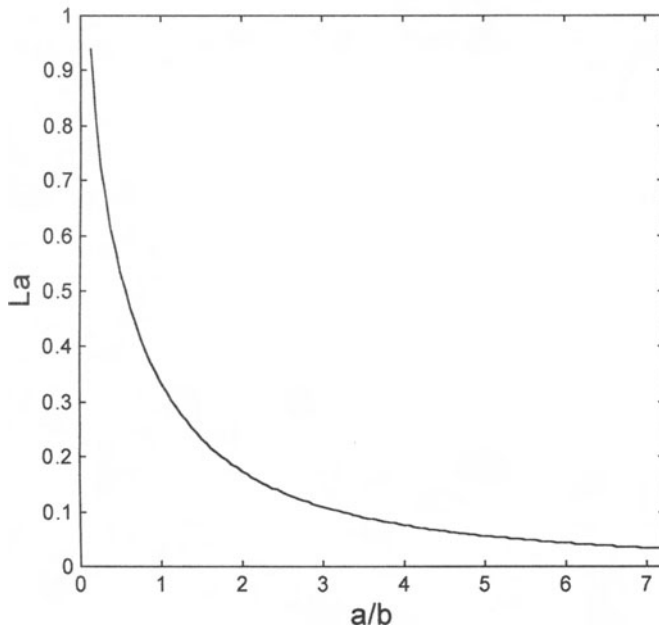
FIGURE 9.12. The depolarization factor in the direction of the a-axis for an ellipsoid of revolution with semi-axes a, b, and c, where b = c.

There are three cases of considerably interest for us: spheres, needle-shaped ellipsoids and disk-like particles. For a needle-shaped ellipsoid or a particle with the shape of a long cylinder with $a = b \ll c$, L_a, L_b and L_c tend to $1/2$, $1/2$ and 0, respectively. For a sphere with $a = b = c$, the depolarization factor $L_a = 1/3$. For a disk-shaped ellipsoid with $a = b \gg c$, L_a, L_b and L_c tend to 0, 0 and 1 respectively (Fricke, 1953). In Fig. 9.12 the depolarization factor L_a is depicted for a spheroid with semi-axes a, b = c.

Maxwell's mixture equation has been experimentally tested by Cole *et al.* (1969) for variously shaped objects. The particles could be spheres, cubes, or cylinders arranged in a cubic or hexagonal array or randomly distributed plates. They found that the Maxwell equation was surprisingly accurate within one percent at concentrations from 30 percent or less to 90 percent.

9.2.3.1.a. Blood

To illustrate the applicability of Maxwell's mixture equation, the conductivity of blood is discussed. Blood of normal subjects consists predominantly of red blood cells (erythrocytes) in plasma. The mature erythrocyte is a cell surrounded by a deformable membrane well adapted to the need to transverse narrow capillaries. The red cells are biconcave disks, each with a diameter of about 8μm, a thickness of 2μm at its edge, and a volume of about 94μm^3. In normal adults, the red cells occupy on the average about 48 percent of the volume of blood of males and about 42 percent in the blood of females. The percentage of the volume of blood made up by erythrocytes is defined as the hematocrit. Erythrocytes are essentially

TABLE 9.7. Parameter values used to estimate the conductivity perpendicular to the fibers and that parallel to the fibers. ([a]Kobayashi and Yonemura, 1967)

parameter	symbol	minimum	maximum
effective intracellular conductivity	σ_i	0.55 S/m	0.80 S/m
extracellular conductivity	σ_e	2.0 S/m	2.4 S/m
membrane conductivity	σ_m	1.0×10^{-8} S/m	1.2×10^{-6} S/m
volume fraction occupied by fibers	p	0.85	0.9[a]
fiber length	L	5 mm	30 cm
membrane thickness	t	0.1 μm	1 μm

non-conducting in fields with frequencies up to 100kHz (Trautman and Newbower, 1983). A typical value for the low-frequency conductivity of human blood at body temperature and normal hematocrit is in the range 0.43–0.76S/m (Geddes and Baker, 1967). The orientation of the ellipsoids with respect to the electric field depends on the blood flow. There is a periodic noise component in continuous measurements of conductivity, which is presumed to result from the cyclic reorientations due to the flow. The magnitude of the change with flow is of the order of three percent of the baseline conductivity. Since the shape of red blood cells of most species is non-spherical and is subject to changes in aggregation and orientation with flow, variations in the effective conductivity are understandable.

Geddes and Sadler (1973) measured the conductivity for human, canine, bovine and equine blood at 25kHz and 37°C, having a hematocrit range extending from 0 to 70 percent. For human blood they found an exponential fit between the measured data and an exponential curve for $\rho = 53.2e^{0.022H}$ with a correlation coefficient of 0.99. Blood can be modeled as a dilute solution of non-conducting spherical particles within a conducting medium. In Fig. 9.7 both the experimental measurements and the results using Maxwell's mixture equation for spherical particles are displayed. From this figure one can conclude that the description of Maxwell is rather accurate. With increasing concentration of red blood cells (p is larger) the effective conductivity is reduced. The relationship between p and the conductivity can be used to estimate the hematocrit content (Ülgen and Sezdi, 1998).

9.2.4 ARCHIE'S LAW

Measurements of the conductivity of the cortex do not fit so well with the theory of Maxwell, they fit better with Archie's law (Archie, 1942; Nicholson and Rice, 1986). Moreover, Maxwell's theory can only be applied if there is only one type of cell present and most human tissues are constituted of various types of cells. Archie's law that will be discussed in the next section is applicable if there are various types of densely-packed non-conducting cells suspended in a conducting solution.

To derive Archie's law the following assumptions are made. a) Tissue is modeled by cells of various shapes that are suspended in an aqueous conducting medium; b) The effective conductivity is calculated for a region containing thousands of particles; c) The particles are assumed to be homogeneously distributed; d) Currents are Ohmic and are only present in the extracellular space; e) The solvent is homogeneous and isotropic; f) An electric field is applied which is initially uniform; g) The particles do not have a permanent electric dipole moment.

9.2.4.1 Ellipsoidal particles with the same orientation

The derivation of an equation for the effective conductivity for higher values of p is given by Hanai (1960). It starts with equation (9.14). Subsequently, the number of particles is increased. Due to this increase, the effective conductivity σ_{eff} increases with a fraction $\Delta\sigma_{eff}$. In the next stage the previous mixture acts as a host, and so on. An expression for the effective conductivity of a densely packed suspension of ellipsoidal particles is obtained by integration yielding:

$$\frac{\sigma_{eff} - \sigma_{part}}{\sigma_e - \sigma_{part}} \left(\frac{\sigma_e}{\sigma_{eff}}\right)^{L_a} = 1 - p \qquad (9.16)$$

Inserting in this equation $\sigma_{part} = 0$ yields Archie's law:

$$\sigma_{eff} = \sigma_e(1 - p)^m \qquad (9.17)$$

where σ_e is the conductivity of the fluid surrounding the non-conducting cells, p is the volume fraction occupied by the cells, and m is the so-called cementation factor that depends on the shape and orientation of the particles, but not on their sizes. According to Archie's law, the effective conductivity is proportional to the extracellular conductivity σ_e. The value of m depends on the shape of the cells. For instance, its value is 3/2 for spherical particles, m is 2 for long cylinders with the axis perpendicular to the external field, and it is 1 for cylinders with the axis parallel to the field. Archie's law also holds for ellipsoidal particles. If the field is applied along the a-axis of the ellipsoids and the ellipsoids have the same orientation,

$$m = 1/(1 - L_a) \qquad (9.18)$$

9.2.4.1.a. Fat

Since fat tissue consists of about 9 percent water (Foster and Schwan, 1989) and the interior of the cells is almost completely filled with fat, the interstitial fluid occupies about 9 percent of the volume (upper limit). Histology shows that fat cells are spherical-shaped particles. According to equation (9.17) an upper limit for the conductivity is $1.9 \times (0.09)^{3/2} \approx 0.05$ S/m.

9.2.4.1.b. Skeletal muscles

A skeletal muscle fiber represents a single cell of muscle. Each skeletal muscle fiber is a thin elongated cylinder with rounded ends that are attached to connective tissues associated with the muscle. Just beneath its cell membrane, the cytoplasm of the fiber contains many small nuclei and mitochondria. The cytoplasm also contains numerous threadlike myofibrils that lie parallel to the cylinder axis. The diameter may vary within muscles, between muscles in the same animals, and between species. Muscle fibers increase in diameter from birth to maturity and also in response to exercise. The length of a fiber may vary between millimeters and several tens of centimeters. The amount of connective tissue relative to muscle fibers is much greater in some muscles than in others and may range from 3 to 30 percent. Connective tissue is composed of collagen fibers, reticular fibers, elastic fibers and several varieties of cells, such as fat cells. There is an increase in elastic tissue with aging. Apart from the

fibers in the tongue, the fibers have no branches. In long muscles, as in the longest muscle in the human body the sartorius (52cm long), the fibers are arranged in parallel. Covering the surface of each muscle fiber is a thin membrane of about $0.1\mu m$ thickness. The model used to describe muscle tissue consists of homogeneously distributed cylinders. So far as connective tissue, blood vessels, and nerve tissue cannot be described by parallel cylinders, their influence will be neglected.

The effective conductivity of one fiber when the field is applied parallel to the axis is according to formula (9.9) dependent on the length of the fiber. Inserting the values of Table 9.7 in formula (9.8) yields 0.25×10^{-5}S/m (short fiber) $< \sigma_{part} < 15 \times 10^{-2}$S/m (long fiber). When the fiber is damaged (for instance, Mc Rae and Esrick (1993) trimmed the fibers) then σ_i may be as high as the effective intracellular conductivity. Currents parallel to the fibers will be in both domains, the intracellular and extracellular space are connected in parallel. The effective conductivity of the muscle tissue will be given by $(1 - p)\, \sigma_{extracell} + p\sigma_{eff}$.

When the current is applied perpendicular to the fibers, the cell can be described as a non-conducting cylinder. The effective conductivity perpendicular to the fibers σ_l according to equation (9.17) will be within the limits $2.0 \times (0.1)^2 \leq \sigma_{l,eff} \leq 2.4 \times (0.15)^2$. Thus the effective conductivity perpendicular to the fibers will be in the range of $0.02 - 0.05$S/m.

9.2.4.1.c. Cardiac tissue

Cardiac cells can be described as cylinders with a diameter of about $15\mu m$ and a length of about $100\mu m$. The currents perpendicular to the fibers will circumvent the fibers. The effective conductivity in the direction perpendicular to the fibers can be calculated using expression (9.17) with m = 2. The volume fraction occupied by the fibers reported by Clerc (1976) is p = 0.7. The conductivity of the extracellular space is assumed to be that of Ringer ($\rho = 69\Omega$cm) yielding a conductivity of 1.4S/m. So the conductivity perpendicular to the fibers is estimated to be $1.4 \times (0.3)^2 = 0.13$S/m. Rush et al. (1963) measured the conductivity of cardiac tissue and found for the conductivity perpendicular to the axis 0.18S/m.

Currents parallel to the fibers will be present both in the extracellular and in the intracellular space. Cardiac cells are joined at their ends by intercalated disks and each cell is connected to its neighbors by gap junctions passing through these disks. Cardiac muscle fibers can be modeled by cylinders that are interconnected by junctions as depicted in Fig. 9.13. All cylinders are homogeneously distributed and are arranged in parallel. The current is applied parallel to the axes, such that the volume between the electrodes used to apply the current contains 10^4 fibers or more. Each cylinder has a length of $100\mu m$ and a radius of $7.5\mu m$. All parameters are chosen conform the parameters chosen by Plonsey and Barr (1986) from literature. These values were measured in mammalian ventricular tissue at a temperature of about $20°C$. The resistance of a junction is $R_j = 0.85 \times 10^6\Omega$. The resistivity of intracellular fluid is 282Ωcm (Chapman and Frye, 1978). Consequently, the resistance of a cylinder with a length of 10^{-2}cm and a diameter of $15\mu m$ of intracellular fluid is

$$(282 \times 10^{-2})/(\pi \times (7.5 \times 10^{-4})^2) = 1.60 \times 10^6\Omega.$$

The junction and the intracellular space are connected in series, so the resistance of a single
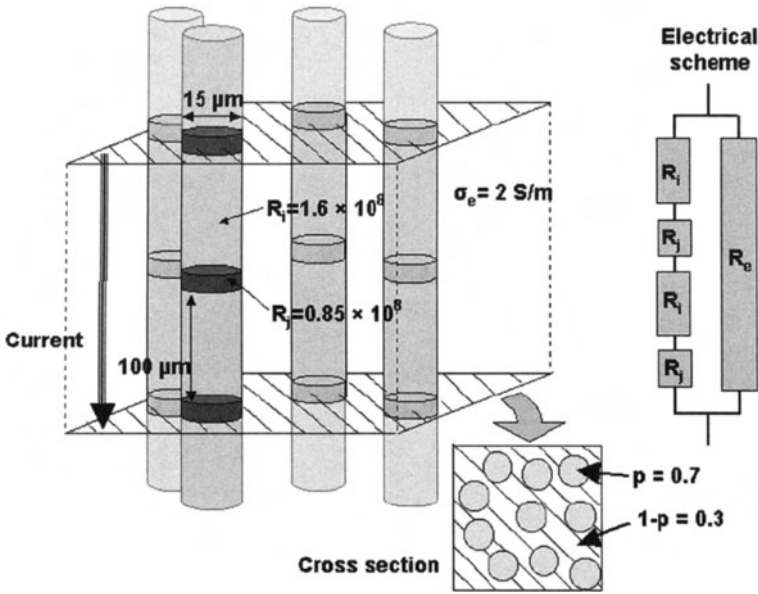
FIGURE 9.13. Model of cardiac tissue.

cylindrical cell is

$$R_{cell} = R_i + R_j = (0.85 + 1.60) \times 10^6 \Omega.$$

A homogeneous cylinder with the same dimensions will have the same resistance R_{cell}, when an effective conductivity σ_{eff} is ascribed to the entire cylinder.

$$\sigma_{eff} = 1/(R_{cell}O), \quad \text{where} \quad l = 10^{-4}m, O = \pi(7.5 \times 10^{-6})^2, \text{ yielding } \sigma_{eff} = 0.23S/m.$$

The two composites of the cardiac tissue, namely the intra- and extracellular medium are connected in parallel. Thus, the effective conductivity along the fibers for cardiac tissue is

$$(1 - p)\sigma_{extracell} + p\sigma_{eff} = 0.3 \times 1.4 + 0.7 \times 0.23 = 0.58S/m.$$

Rush *et al.* (1963) found for the conductivity parallel to the axis of cardiac fibers a value of 0.4S/m.

9.2.4.2 Randomly orientated ellipsoidal particles

The architecture of human tissue may be such that fibers and cells are oriented along each other. For instance, skeletal muscle fibers are more or less parallel. However, the assumption that the cells or fibers have the same orientation is often not plausible. For example, the red blood cells in blood outside of the body can roughly be described by oblate
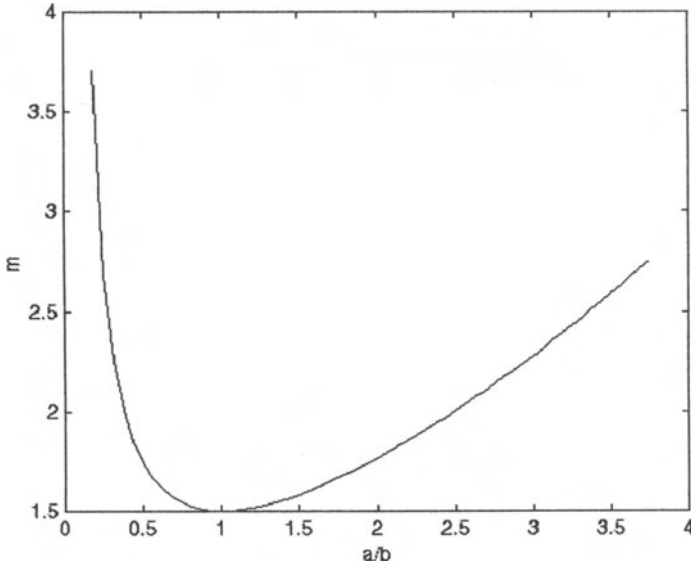
FIGURE 9.14. The cementation factor for a solution of randomly orientated spheroids with semi-axes a, b, and c, where b = c.

spheroids (ellipsoids with a < b = c) that are randomly oriented. Boned and Peyrelasse (1983) derived an expression for a solution of randomly orientated ellipsoidal particles. Every orientation of the particle has the same probability and therefore the Hanai procedure is performed such that infinitesimal amounts of particles are added such that 1/3 of the ellipsoids have their a-axes in the direction of the electric field, 1/3 their b-axes and 1/3 their c-axes. For non-conducting particles again Archie's law is found with a cementation factor

$$m = \frac{1}{3} \sum_{j=a}^{c} \frac{1}{1 - L_j} \tag{9.19}$$

The low-frequency conductivity of suspensions of ellipsoidal particles and that of doublet-shaped (budding yeast cells) or biconcave particles (erythrocytes) differs only a few percent as can be concluded from simulation studies using as numerical method the boundary element method (Sekine, 2000).

In Fig. 9.14 the cementation factor is depicted for an ellipsoid of revolution with semi-axes a, b and c, where b = c. As can be seen m is minimal for $L_a = 1/3$, the depolarization factor for a sphere, in that case σ_{eff} is maximal.

9.2.4.2.a. Blood

Archie's law can be applicated for blood. Fitting the measured data for human blood of Geddes and Sadler (1973) to Archie's law leads to a fit for m = 1.46 (see Fig. 9.7). For blood of different animals, a slightly different cementation factor is found.

9.2.4.3 Cells of different shape

Human tissue can often be described by particles of different shapes that are immersed in an aqueous medium. The cortex, for instance, has pyramidal cells and glial cells. The sizes of the particles do not play a role in the theory derived. A different shaped ellipsoidal particle is one that has a different ratio of the radii along the three axes. In order to obtain an expression for a suspension of particles of different shapes, we applied the Hanai procedure by adding successively infinitesimal numbers of particles in proportion to their relative volume fractions, leading again to Archie's law

$$\sigma_{\text{eff}} = \sigma_{\text{e}} (1 - p)^{m}; \quad \text{with} \quad m = \sum_{i=1}^{n} m_i \frac{p_i}{p} \quad \text{and} \quad m_i = \frac{1}{3} \left(\sum_{j=a}^{c} \frac{1}{1 - L_j} \right) \qquad (9.20)$$

where n is the number of types of non-conducting ellipsoids, p_i the volume fraction of a particle of type i, p the sum of all volume fractions occupied by particles and L_j the depolarization factor in the direction of one of the axes (Peters *et al.*, 2001).

9.2.4.3.a. Gray matter

As an example, the effective conductivity of the superficial cortex is estimated, using parameters found in the literature. The principal neuron types in superficial cortex are pyramidal cells in layer II and stellate cells in layer III. Axons and dendrites from deeper layers and axons from subcortical layers occupy a substantial portion of the tissue. The glial cells of superficial cortex are mostly star-shaped cells, *i.e.* astrocytes and a lesser fraction of oligondendrocytes. The latter resemble astrocytes, but are smaller and have fewer processes. A branching astrocyte process has a length of about 40 microns and an average diameter of about one micron. The shape of the glial cell body *in vitro* is an intermediate between a flat disk and a sphere. The pyramidal cells have a cell body and dendrites. The cell body has a roughly pyramidal shape. The branching properties of dendrites of neurons show a mean branching angle of about 60 degrees. The diameter of motoneurons is reported as 7 to 14μm for the proximal segment with decreasing values of about 5, 3, and 2μm for successive branches. The fact that solutes of high molecular weight readily pass between cerebrospinal fluid (CSF) and interstitial fluid supports the supposition that no significant concentration gradients exist between the two compartments in the steady state. Hence the CSF reflects the ionic composition of the interstitial fluid and the conductivity of the CSF will be identical to that of the interstitial fluid *i.e.*1.8S/m (Baumann *et al.*, 1997).

The gray matter is composed of glial cells that are modeled as spheres, occupying a volume fraction of 38 percent and pyramidal cells that are modeled as cylinders, occupying a volume fraction of 46 percent (Havstad, 1967). Both neurons and glial cells are described by non-conducting particles, *i.e.* $\sigma_{\text{particle}} = 0$. The effective conductivity is computed using equation (9.20) yielding $\sigma_{\text{eff}} = 0.097$S/m. A measurement that used a uniform current to determine the conductivity of gray matter has been carried out by Ludt and Hermann (1973), who reported a value of 0.10S/m for the rabbit. However, the measurements were carried out *in vitro* 15 minutes after death and at room temperature. As found by van Harreveld and Ochs (1956), the conductivity drops after circulatory arrest by 30 to 35 percent due to the emptying of blood vessels and drainage of fluid. Thus Ludt and Hermann's

measurements indicate that the effective conductivity of cortical tissue *in vivo* will be about 0.15S/m. Archie's law led to a value of about 0.10S/m. However, the values used for the calculation may be not optimal. The volume fraction occupied by the extracellular fluid is in the range 17 to 28 percent (van Harreveld *et al.*, 1965; Nicholson and Rice, 1986). The interstitial space and the vascular volume together constitute the extracellular space. The vascular space has a volume of about 1 to 3 percent. So the value of $(1 - p)$ in practice will be somewhat higher than the value handled by us in the computation of the effective conductivity.

9.2.4.4 Clustered cells

When spherical particles are clustered in a chain or in a close-packed lattice, the conductivity is such that these clusters behave as randomly orientated ellipsoids and thus Archie's law will be obeyed (Grandqvist and Hunderi, 1978).

9.2.4.4.a. Blood

Blood with a high hematocrit content may aggregate. Pfützner (1987) measured the conductivity of blood samples containing red blood cells of varying diameter between 100Hz and 100kHz. The conductivity was essentially independent of the diameter of the cells and the frequency. He found that at a hematocrit of 60 percent or more that the dielectric constant shows a distinct decrease. This was explained by the aggregation of blood cells. An aggregation in a single cell chain, for instance, would lead to effective depolarization factors $L_a = 0.13$; $L_b = L_c = 0.435$, leading according relation (9.19) to m = 1.6. In such case, the effective conductivity at 80 percent hematocrit would practically be the same as without aggregation (2 percent difference).

9.2.4.4.b. Liver

The liver consists of different types of cells. These can be divided in hepatocytes and non-hepatocytes (Raicu *et al.*, 1998[a]). But since the volume fraction of non-hepatocytes (0.06) is relatively small to that of the hepatocytes (0.72) a model is used consisting of one cell-type. The hepatic cells are clustered forming plates of one layer in thickness (see Fig. 9.15). The close-packed clusters of cells are assumed to act as oblate spheroids with axes

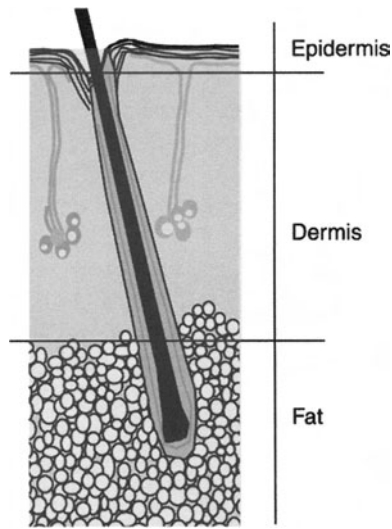**FIGURE 9.15.** A schematic drawing of a part of a lobule of the liver.

FIGURE 9.16. A schematic drawing of the layered human skin.

a, b, c, where a $=$ b $\gg$ c. Choosing the effective depolarization factors L_a, L_b, and L_c to be $0.1, 0.1$ and 0.8, respectively and applying Archie's law with p $= 0.72$ and $\sigma_s = 0.65 S/m$ (the conductivity of blood) results in $\sigma_{eff} = 0.03 S/m$. This finding is in accordance with findings of Gabriel *et al.* (1996[a]) who reported values in the range of 0.02–$0.03 S/m$. Choosing L_a, L_b, and L_c to be 0.2, 0.2 and 0.6 leads to an effective conductivity of $\sigma_{eff} = 0.08 S/m$, which is more in accordance with the values given by Geddes and Baker (1967) and Raicu *et al.* (1998[b]).

9.3 LAYERED STRUCTURES

Many tissues are organized in layers, such as the gastrointestinal tract, the retina, or the gray matter. An example of a layered structure is shown in Fig. 9.16, where the scalp is depicted. At an interface current lines will change direction. Coming from a medium with higher conductivity to a medium with lower conductivity, current lines will bend in the direction of the normal. Coming from a medium with lower conductivity to a medium with higher conductivity, current lines will bend from the normal. As a consequence, currents tend to cross the skull in a direction perpendicular to its surface. In other words, the layers of the skull are approximately traversed in series. Currents in the scalp tend to be parallel to its surface and the layers of the scalp can be approximated by a parallel connection of resistances. The simulations discussed in sections 3a and 3b show that this is indeed the case.

9.3.1 THE SCALP

The outer layer of the scalp is the epidermis of about 0.2mm thickness. This layer is non-sensitive and non-vascular and overlies the dermis. The epidermis is a poorly conductive

layer; this is ascribed to the dead nature of one of the layers within the epidermis, the stratum corneum. The conductivity of the epidermis is approximately 0.026S/m (Semrov *et al.*, 1997). The dermis is connective tissue with a thickness of 2mm and its conductivity is estimated to be 0.22S/m (Yamanoto and Yamanoto, 1976). The basis of the dermis is a supporting matrix with a remarkable capacity for holding water. The dermis has a very rich blood supply. At the side of the head, subcutaneous fat is found of about 3mm thickness. Semrov *et al.* (1997) used a conductivity value of 0.08S/m for this layer.

To assess the effective conductivity of the scalp, a simulation is performed with a spherical volume conductor. Two models are used. The first model consists of five shells representing the brain, skull, fat layer (3mm), dermis (2mm) and the epidermis (0.2mm). The conductivities of the three layers are mentioned above. The radii and conductivity of the brain and skull are 78 and 83mm, and 0.33 and 0.0042S/m, respectively. The other model has 3 shells: the brain, skull and the skin. The radii and conductivities of the brain and skull are equal to those of the first model. The thickness of the skin layer is chosen to be the sum of the thickness of the fat layer, dermis and epidermis. The effective conductivity of the entire skin layer is calculated (assuming that the currents are crossing the scalp such that the layers are approximately connected in parallel) by means of

$$\sigma_{\text{eff,scalp}} = \frac{\sum_{i=1}^{3} d_i \sigma_i}{\sum_{i=1}^{3} d_i} \tag{9.21}$$

where d_i and σ_i denote the thickness and conductivity of layer i. This yields a value of 0.13S/m for the effective conductivity of the skin. A current dipole on the z-axis is used as source. The potential is calculated at the outer sphere by means of an analytical expression (Burik, 1999). The potential using the three-shell model is compared with the potential using the other five-shell model. The differences are expressed by the relative difference measure (RDM) defined as

$$\text{RDM} = \sqrt{\frac{\sum_{i=1}^{N} (V_i - V_{c,i})^2}{\sum_{i=1}^{N} V_{c,i}^2}} \tag{9.22}$$

where V_i is the calculated value of the potential for the three-shell model, $V_{c,i}$ is the calculated value of the potential for the five-shell model and N is the number of points were the values are calculated. The calculations are repeated varying the eccentricities and orientations of the dipole, and the ratio of the thickness of the three layers of the skin. Some results are shown in Fig. 9.17. It can be seen that equation (9.21) can be used to calculate the effective conductivity of the scalp when the thickness of the various layers is known. If these thicknesses are not known then $\sigma = 0.13$S/m will be an appropriate choice for the effective conductivity of the scalp.

9.3.2 THE SKULL

Another example of a layered structure is the skull that can also be subdivided into three layers. The upper and lower layers are structures made out of bone, which are bad conductors. The middle layer is a relatively good conductor, because it is spongy and
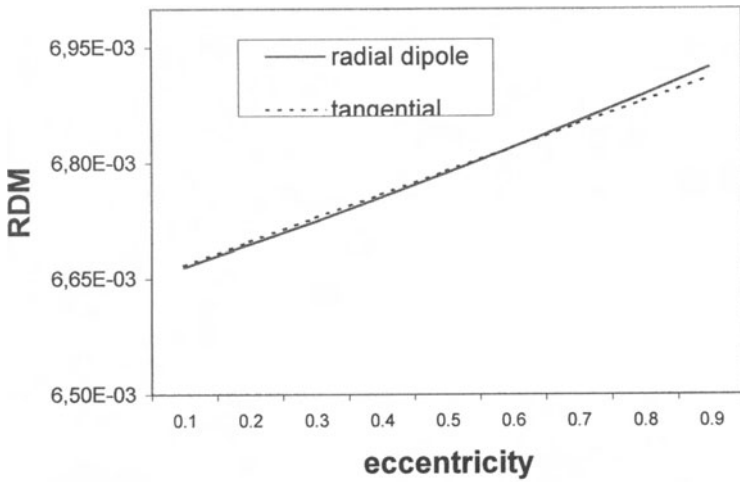
FIGURE 9.17. The RDM between the scalp potential calculated using an effective conductivity and the one calculated for a skin composed of 3 layers, namely the epidermis, the dermis and the fat.

contains blood. The total thickness varies across the skull between 4 and 11mm, the mean is around 6mm. The skull has a conductivity in the direction perpendicular to the surface of a factor 10 smaller than in the direction parallel to the surface. Usually, a value of 0.0042S/m is assigned to the conductivity of the entire skull, although recent measurements of the conductivity of the skull using bone that was temporarily removed during epilepsy surgery led to values that were a factor ten higher (Hoekema *et al.*, 2001).

Simulations are performed with a spherical volume conductor. The volume conductor consisting of the brain, skull and scalp is modelled by either a three-shell model in which an effective conductivity is assigned to the skull or a five-shell model. The radii and conductivity of the brain and scalp are 78 and 89.2 mm, and 0.33 and 0.13S/m, respectively. The skull is described by three layers of conductivity of 0.0029, 0.029 and 0.0029S/m, respectively. These values are chosen such that for a mean skull thickness of 6mm consisting of layers of 2mm each, the effective conductivity is 0.0042S/m.

The other model has 3 shells: the brain, skull and the scalp. The radii and conductivities of the brain and scalp are equal to those of the first model. The thickness of the skull is varied between 2 and 10mm. The ratio between the thicknesses of the three layers describing the skull is varied as well. A current dipole is taken as the source, whose position and orientation are varied. As the conductivity of the skull is much lower than that of the surrounding tissues one may expect that the currents will cross the skull perpendicularly. This implies that the three layers of the skull are crossed in series. If the effective conductivity is given by

$$\left(\frac{1}{\sigma}\right)_{\text{eff,skull}} = \frac{\sum_{i=1}^{3} \dfrac{d_i}{\sigma_i}}{\sum_{i=1}^{3} d_i} \qquad (9.23)$$

then the RDM is well below 2 percent. Hence, we may conclude that the effective

conductivity of the skull is approximated quite well by expression (9.23). When realistically-shaped models are used in the inverse solution, both the thickness and the conductivity should vary.

9.3.3 A LAYER OF SKELETAL MUSCLE

In the ECG inverse problem the muscle layer may be considered as one of the compartments. Some simulation studies suggest that this anisotropic layer is the only thoracic inhomogeneity with a significant effect on the relationship between epicardial and torso potentials (Stanley *et al.*, 1991). The muscles underneath the skin of the torso are essentially directed parallel to the body surface but otherwise almost uniformly distributed over all angles(Rush, 1967). This implies that the conductivity parallel to the body surface differs from that perpendicular to it. Half of the fibers that are parallel to the body surface are perpendicular to the other half. The conductivity parallel to the body surface will be about $\sigma_m = (\sigma_l + \sigma_h)/2$. The conductivity perpendicular to the body surface is σ_l. We choose a co-ordinate system such that $\sigma_x = \sigma_y = \sigma_m$ and $\sigma_z = \sigma_l$.

Expression (9.2) reads in this case:

$$\left(\sigma_m \frac{\partial^2}{\partial x^2} + \sigma_m \frac{\partial^2}{\partial y^2} + \sigma_l \frac{\partial^2}{\partial z^2} \right) V = 0 \qquad (9.24)$$

If the muscle layer is modeled as layer of infinite extent with thickness t, then the proper boundary conditions are that at the surface the normal component of the current density is continuous and the potential is continuous.

Equation (9.24) can be solved by a co-ordinate transformation from (x,y,z) to (x',y',z'), where

$$x' = x; y' = y \quad \text{and} \quad z' = z\sqrt{\sigma_m/\sigma_l} \qquad (9.25)$$

The scale transformation is such that the currents and the potential are chosen to be invariant. In other words they are the same at corresponding points of the primed and unprimed system. The components of the current density being a current divided by a surface transform as:

$$j'_x = j_x\sqrt{\sigma_m/\sigma_l}; \qquad j'_y = j_y\sqrt{\sigma_m/\sigma_l} \qquad \text{and} \qquad j'_z = j_z \qquad (9.26)$$

The electric field being the gradient of the potential transforms as:

$$E'_x = E_x; \quad E'_y = E_y \quad \text{and} \quad E'_z = E_z\sqrt{\sigma_m/\sigma_l} \qquad (9.27)$$

As a consequence, in the primed system:

$$\nabla^{2'}V' = 0 \quad \text{and} \quad \vec{j}' = \sqrt{\sigma_m\sigma_l}\vec{E} \qquad (9.28)$$

Hence, after transformation we have to solve Laplace's equation with the proper boundary condition (*i.e.* the z-component of the current density is continuous), which is invariant under the co-ordinate transformation. The primed system is isotropic with conductivity

$\sqrt{\sigma_m \sigma_l}$. In other words, the potential of the anisotropic muscle layer is equivalent to the potential in a homogeneous isotropic medium with an effective conductivity $\sqrt{\sigma_m \sigma_l}$, if the thickness is enhanced with a factor $\sqrt{\sigma_m/\sigma_l}$.

Inserting $\sigma_l = 0.05 S/m$, $\sigma_h = 0.5 S/m$ for skeletal muscle and taking a layer thickness $t = 1 cm$ yields for the effective conductivity of the muscle layer $\sigma_{eff} \approx 0.11 S/m$ and an effective thickness of the muscle layer of 5cm.

Stanley *et al.* (1986) showed that the agreement between calculated and measured torso potentials significantly improved if the anisotropic nature of the muscle layer was taken into account. Their results were based on a canine study.

9.4 COMPARTMENTS

Customarily, the volume conductor is described by a compartment model. Each compartment is considered to be homogeneous. The number of compartments may vary. To solve the inverse problem for EEG, the head is often described by three compartments, the brain, skull and scalp. Usually, the conductivity assigned to the brain and to the scalp compartment are identical. The geometry of these compartments may be a sphere covered by two spherical shells or the compartments may have a realistic shape. Especially in the case that a three-sphere model of the head is used with standard radii of the spheres, the interfaces between the compartments will not coincide with the actual interfaces between the different tissues. Consequently, a compartment will consist of more than one type of tissue. For instance, the muscles that are present in the occipital and orbito-frontal areas of the scalp may be partly assigned to the scalp compartment and partly to the skull compartment. The cerebrospinal fluid may be assigned mainly to the brain compartment, but also partly to the skull compartment. Consequently, the effective conductivities do not represent the actual conductivities of brain matter, skull bone or skin. The effective conductivities are those values that minimize the differences between the actual EEG and the calculated EEG.

The effective conductivity of a compartment can be estimated in three ways. First, implanted electrodes can be used to act as a source. Measurements of the potential or magnetic field distribution generated by the source can be used to estimate the source. The actual source can be compared with the calculated one. By varying the effective conductivities used in the models the differences between the actual source and the calculated one can be minimized. The conductivities that give the smallest differences are taken as the effective ones. Second, the effective conductivities can be determined by fitting evoked magnetic field measurements with those of the electrical potential in case that the potentials and magnetic fields are due to the same source. The third method is based on impedance tomography.

9.4.1 USING IMPLANTED ELECTRODES

Sometimes electrodes are inserted in the brain through trephine holes during presurgical evaluation of epileptic patients (Veelen *et al.*, 1990). Normally, these electrodes are used for the measurement of the potential, especially during long term seizure monitoring. However, when a current is applied to a pair of electrodes, it will act as an artificial source. Its location and orientation is known from X-ray or magnetic resonance images. The artificial source can be localized from potential measurements on the scalp. The true and calculated

location should coincide. This can be established by varying parameters of the model used in the inverse solution, such as the ratio between the conductivities in a three-compartment model of the head. Homma *et al.* (1994) used a realistically shaped model and found that the inverse solution was the best when the ratio between the conductivities was $1 : 1/80 : 1$.

9.4.2 COMBINING MEASUREMENTS OF THE POTENTIAL AND THE MAGNETIC FIELD

Cohen and Cuffin (1983) measured magnetic fields and electrical potentials that were evoked by the same stimulus. Both types of measurements were used to localize a dipole within a standard three-sphere model of the head. The locations coincided when using the ratio $1 : 1/80 : 1$ for the equivalent conductivity of the brain, the skull, and the scalp compartment. Gonçalves *et al.* (2001) repeated these measurements in four subjects. They reported values for the conductivity ratio between scalp and skull that varied between 43 and 85. Part of the observed variability may be ascribed to errors in the volume conductor model, numerical errors, or errors in the measurement. The effect of these errors on the potential distribution will differ from that on the magnetic field distribution. Part will be due to the differences between the heads of the four individuals. In each head the distribution of inhomogeneities within compartments will be different.

9.4.3 ESTIMATION OF THE EQUIVALENT CONDUCTIVITY USING IMPEDANCE TOMOGRAPHY

When a current is applied to the scalp surface, a potential distribution develops across the head. The relation between the applied currents and the resulting potential depends on the conductivity distribution within the head. The distribution of the internal conductivity can be estimated from measurements of this scalp potential. This type of research is known as electrical impedance tomography. Gonçalves *et al.* (2001) used electrical impedance tomography to estimate the ratio between the effective conductivity of the skull and the brain compartment for five subjects under the condition that the brain has the same effective conductivity as the scalp. They used both a spherical and a realistically-shaped three-compartment model. For the spherical model they found for the ratio of the brain and scalp conductivities values that varied between 31 and 124. They ascribed the observed variability to geometrical errors. Differences between the actual head geometry and the three-compartment model are compensated by adjusting the values of the electrical conductivity of the compartments. These errors will be much smaller in case realistically-shaped models are used. And indeed for their realistically-shaped models the spread is decreased. In the latter case the ratio of the effective conductivity of brain and skull varied between 17 and 65. They suggest that electrical impedance tomography should be a part of the EEG inverse problem in order to take the individual differences in effective conductivities into account. Oostendorp *et al.* (2000) used this method to estimate the effective conductivity of the skull and scalp compartment for two subjects. Fitting their potential measurements to the potentials computed by means of the boundary element method yielded a skull conductivity of $0.013 S/m$ and a brain conductivity of $0.20 S/m$. The value found for the ratio of brain-to-skull conductivity was $15 : 1$.

Impedance tomography can also be used to estimate the effective conductivities used in a compartment model of the torso. Eyüboğlu *et al.* (1994) used this method to estimate the effective conductivities of the heart, lungs and body in a dog. However, the accuracy of the estimated effective conductivities was only about 40 percent, because the method is not sensitive for changes in conductivities in the various compartments.

9.5 UPPER AND LOWER BOUNDS

In most cases, it is very difficult to actually calculate the effective conductivity of a composite material because of lack of detailed information on the micro-geometric structure. Based on information available, lower and upper bounds for the effective conductivity can be given. The range between these bounds decreases with increasing knowledge about the constituents of the composite medium.

The conductivity of a composite medium cannot be higher than that of the best conducting phase and cannot not be lower than the worst conducting phase. Thus, for a material consisting of n phases, denoted by the index $i = 1, 2, 3, \ldots, n$, with σ_i increasing with i, the limits are

$$\sigma_1 \leq \sigma_{\text{eff}} \leq \sigma_n \tag{9.29}$$

Stricter bounds are found when apart from the conductivities also the volume fractions p_i of all phases are known. These bounds read (Hashin and Shtrikman, 1962)

$$\left(\sum_{i=1}^{n} \frac{p_i}{\sigma_i} \right)^{-1} \leq \sigma_{\text{eff}} \leq \sum_{i=1}^{n} p_i \sigma_i \tag{9.30}$$

The upper bound is, for instance, attained for a two-phase composite medium consisting of a suspension of needle-shaped particles with the applied field in the direction of their principal axes. The lower bound is, for instance, attained for a suspension of thin disks that are stacked and the field is applied perpendicular to the disks.

In case it is known that the distribution of the constituents is homogeneous and the medium is isotropic, more rigorous limits are applicable (Hashin and Shtrikman, 1962). In this case, the upper and lower bound for a two-phase material is given by:

$$\sigma_1 + \frac{p_2}{\dfrac{1}{\sigma_2 - \sigma_1} + \dfrac{p_1}{3\sigma_1}} \leq \sigma_{\text{eff}} \leq \sigma_2 + \frac{p_1}{\dfrac{1}{\sigma_1 - \sigma_2} + \dfrac{p_2}{3\sigma_2}} \tag{9.31}$$

If the composite constitutes of homogeneously distributed and randomly orientated particles within a conducting medium, and the particles are non-conducting spheroids $(L_b = L_c)$, the upper and lower bounds can be obtained from Archie's law. The depolarization factors are restrained to $L_a + L_b + L_c = 1$ and $L_a > 0, L_b > 0, L_c > 0$.

According to expression (9.19), the cementation factor m in Archie's law reads in this case:

$$m = \frac{1}{3} \left(\frac{1}{1 - L_a} + \frac{2}{1 - L_b} \right) = \frac{1}{3} \left(\frac{1}{1 - L_a} + \frac{4}{1 + L_a} \right) \tag{9.32}$$

The maximum effective conductivity is found when

$$\frac{\partial \sigma_{\text{eff}}}{\partial L_a} = \sigma_{\text{solv}}(1 - p)^m \ln(1 - p)\frac{\partial m}{\partial L_a} = 0 \qquad (9.33)$$

yielding an upper bound for $L_a = L_b = L_c = 1/3$

$$\sigma_{\text{eff}} \leq \sigma_{\text{solv}}(1 - p)^{3/2} \qquad (9.34)$$

In other words, the upper bound is attained when the particles are spheres. Apparently, such a suspension has the least impact on the flow of currents through the material. The lower bound $\sigma_{\text{eff}} = 0$ is attained when the particles are thin disks ($L_a = 1, L_b = L_c = 0$). Often the ratio between the axes of the spheroidal particles is not known, but it is known that a > b = c. In that case the lower bound is found for cylinders, where $L_a = 0, L_b = L_c = 1/2$, leading to

$$\sigma_{\text{solv}}(1 - p)^{5/3} \leq \sigma_{\text{eff}} \qquad (9.35)$$

In summary, for elongated, homogeneously distributed and randomly oriented non-conducting spheroids in suspension the effective conductivity is limited by the following bounds

$$\sigma_{\text{solv}}(1 - p)^{5/3} \leq \sigma_{\text{eff}} \leq \sigma_{\text{solv}}(1 - p)^{3/2} \qquad (9.36)$$

In Fig. 9.18 the various upper and lower bounds are plotted for a two-phase composite medium consisting of a non-conducting phase embedded in a conducting medium as a function of the volume fraction occupied by the non-conducting phase.

9.5.1 WHITE MATTER

White matter appears white because it contains fiber groups that possess myelin sheaths that consist of layers of membranes. These membranes, composed largely of a lipoprotein called myelin, have a higher proportion of lipid than other surface membranes. The oligodendrocytes (i.e. star-shaped cells) are arranged in rows parallel to the myelinated nerve fibers, with long processes running in the same direction. The white matter can be modeled as a suspension of elongated particles that may have any direction. The extracellular space measured by van Harreveld and Ochs (1956) in the cerebellum of mice varied between 18.1 and 25.5 percent with a mean of 23.6 percent. The conductivity of the interstitial fluid is that of the cerebrospinal fluid, i.e.1.8S/m. Thus according to equation (9.36), the effective conductivity will be between the limits $0.10\text{S/m} < \sigma_{\text{eff}} < 0.23\text{S/m}$.

9.5.2 THE FETUS

In order to simulate the fetal electrocardiogram, a single compartment may describe the fetus. As no measured values for the conductivity of the human fetus are available, its conductivity is estimated. In order to be able to use the theory presented above, the
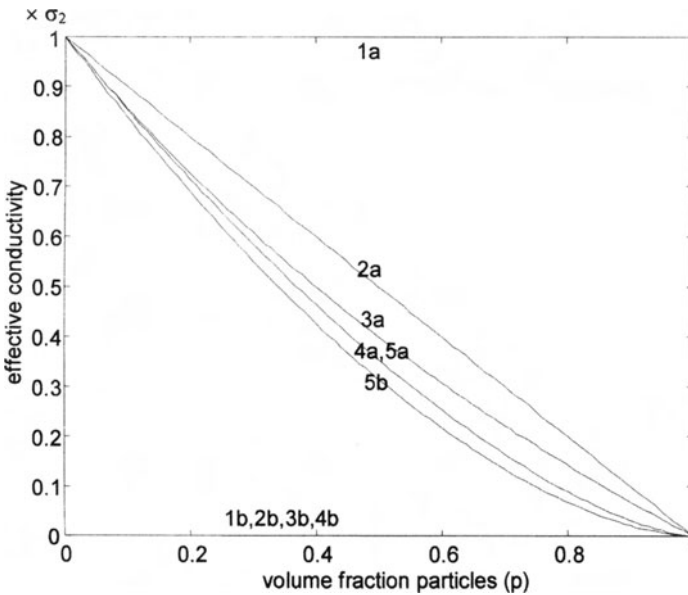
FIGURE 9.18. Upper and lower bounds for a material consisting of two composites where one phase is non-conducting as a function of the volume fraction occupied by the non-conducting phase. The conductivity of the conducting phase is σ_2.
(1a) Upper bound if the only information that is available is the value of σ_2; the lower bound (1b) coincides with the x-axis.
(2a) upper bound and (2b) lower bound if the only information that is available is the value of σ_2 and the volume fraction p.
(3a) upper bound, (3b) lower bound if the phases are homogeneously distributed and σ_2 and p are known.
(4a) upper bound and (4b) lower bound if the non-conducting phase consists of spheroidal, homogeneously distributed particles and the values of σ_2 and p are known.
(5a) upper bound and (5b) lower bound if the non-conducting phase consists of elongated particles that are homogeneously distributed and randomly orientated and the values of σ_2 and p are known.

fetus is assumed to be a homogeneous conductor. It is assumed that the cells in the fetus are homogeneously distributed and randomly orientated and have a shape somewhere between a sphere and a cylinder. Looking at the histology of the fetus most tissues consist of elongated spheroids or spheres. Disc-like cells are less commonly encountered. Based on these assumptions the conductivity of the fetus can be estimated to be between the limits $\sigma_e(1 - p)^{5/3} \leq \sigma_{fetus} \leq \sigma_e(1 - p)^{3/2}$. The volume fraction of the extracellular space at the end of gestation is about 40 percent of the total body volume (Brace, 1998; Costarino and Brans, 1998). The extracellular space includes besides the interstitial fluid the fluids in the body cavities like the cerebrospinal fluid and the blood plasma. The blood plasma is about 18 percent of the total extracellular water content. As the fetus is considered as one single entity, there is no objection in taking all the extracellular fluid in account in estimating the conductivity, as all contribute to the conductivity. In comparison the extracellular fluid fraction in an adult is about 20 percent. Thence, the fetus is at least a factor two more conducting than the maternal abdomen. Assuming the conductivity of the extracellular space in both fetus and adult to be comparable at a value of 2S/m, equation (9.36) predicts a range

of $1.9 \times (0.4)^{5/3} \approx 0.41 \mathrm{S/m} \leq \sigma_{\mathrm{fetus}} \leq 1.9 \times (0.6)^{3/2} \approx 0.88 \mathrm{S/m}$. Assuming that the volume fraction will be somewhere between 40 and 60 percent and will approach 40 percent at the end of gestation, a value of 0.5S/m is a reasonable choice for the conductivity of the fetus in the third trimester of pregnancy. This value is used for the solution of the inverse problem for fetal ECG and leads to reasonable results (Stinstra, 2001).

9.6 DISCUSSION

The accuracy of measurements will be limited because the measurements are very complicated. The accuracy of the computation is limited because the cells vary in shape, they are not homogeneously distributed, blood supply plays a role, etcetera. Since the model used to describe a tissue in this chapter is a simplification the results are only an approximation. However, the results are useful in clarifying the relation between the conductivity and the structure of the tissue. The results can be used to predict the effects of changes due to, for instance, temperature, illnesses or age. Anyhow, it makes no sense to use values of the effective conductivity that suggest an accuracy higher than ten percent by giving the values with too many digits.

The effective electrical conductivity is a macroscopic parameter that represents the electrical conductivity of the tissue averaged in space over many cells. Many of the tissues in the body such as lung, liver, fat, and blood have cells structures that macroscopically show no preferred direction. Even the heart, which is muscular, has its muscle strands wound in such a complicated fashion that, overall, no preferred direction can be readily discerned. Baynham and Knisley (1999) measured the effective epicardial resistance of rabbit ventricles and found that in contrast to isolated fibers the ventricular epicardium exhibits an isotropic effective resistance due to transmural rotation of fibers. Only skeletal muscle cells have a definite preferred direction when many cells are averaged (Rush *et al.*, 1984). Most cells have an elongated shape. Thence, the bounds given in section 9.5 can be used to estimate the effective conductivity. These bounds are not so far apart, so they will help to restrict the uncertainties in the effective conductivity to be used in the bioelectrical inverse problem. An exception form long skeletal muscle and heart tissue, as the conductivity parallel to the fibers will take place both in the extracellular and the intracellular space.

REFERENCES

Archie, G.E., 1942, The electrical resistivity log as an aid in determining some reservoir characteristics, *Trans. Am. Institut. Min. Metal. Eng.*, **146**: 55–62.

Aseyev, 1998, Electrolytes. Interparticle interactions. *Theory, calculation methods and experimental data,* Begell House inc., New York.

Baumann, S.B., Wozny, D.R., Kelly, S.K., and Meno, F.M., 1997, The electrical conductivity of human cerebrospinal fluid at body temperature, *IEEE T. Bio-Med. Eng.*, **44**: 220–223.

Baynham, C.T., Knisley, S.B., 1999, Effective resistance of rabbit ventricles, *Ann. of Biomed. Eng.*, **27**: 96–102.

Boned, C., and Peyrelasse, J., 1983, Etude de la permittivite complexe d'ellipsoïdes disperses dans un milieu continu. Analyses theorique et numerique, *Colloid Polym. Sci.*, **261**:600–612.

Boyle, M. H., 1985, The electrical properties of heterogeneous mixtures containing an oriented spheroidal dispersed phase, *Colloid Polym. Sci.*, **263**:51–57.

Brace, R.A., 1998, Fluid distribution in the fetus and neonate, in: *Fetal and neonatal Physiology*. (R. A. Polin, and W.W. Fox, eds.), Saunders Comp., Philadelphia, pp. 1703–1713.

Burger, H. C., and Dongen, R. van, 1961, Specific electric resistance of body tissues, *Phys. Med. Biol.*, **5**: 431–437.

Burger, H. C., and Milaan, J. B. van, 1943, Measurement of the specific resistance of the human body to direct current, *Act. Med. Scand.*, **114**:585–607.

Burik, M. J. van, 1999, Physical aspects of EEG, PhD thesis, University of Twente, the Netherlands.

Chapman, R.A., and Frye, C.H., 1978, An analysis of the cable properties of frog ventricular myocardium, *J. Physiol.*, **283**:263–283.

Clerc, L., 1976, Directional differences of impulse spread in trabecular muscle from mammalian heart, *Ibid*, **255**:335–346.

Cohen, D., and Cuffin, B.N., 1983, Demonstration of useful differences between magnetoencephalogram and electroencephalogram, *Electroen. clin. Neuro.*, **56**:38–51.

Cole, K. S., Li, C., and Bak, A. F., 1969, Electrical analogues for tissues, *Exp. Neurol.*, **24**:459–473.

Costarino, A.T., and Brans, Y. W., 1998, Fetal and neonatal body fluid composition with reference to growth and development, in: *Fetal and neonatal Physiology*, (R. A. Polin, and W.W. Fox, eds.), Saunders Comp., Philadelphia, pp. 1713–1721.

De Luca, F., Cametti, C., Zimatore, G., Maraviglia, B., and Pachi, A., 1996, Use of low-frequency electrical impedance measurements to determine phospholipid content in amniotic fluid, *Phys. Med. Biol.*, **41**:1863–1869.

Epstein, B. R., and Foster, K. R., 1983, Anisotropy in the dielectric properties of skeletal muscle, *Med. Biol. Eng. Comput.*, **21**:51–55.

Eyüboğlu, B. M., Pilkington, T. C., and Wolf, P. D., 1994, Estimation of tissue resistivies from multiple-electrode measurements, *Phys. Med. Biol.* **39**:1–17.

Foster, K. R., and Schwan, H. P., 1989, Dielectric properties of issues and biological materials: a critical review, *Crit. Rev. Biomed. Eng.*, **17**:25–104.

Foster, K. R., and Schwan, H. P., 1986, Dielectric permittivity and electrical conductivity of biological materials, in: *Handbook of Biological Effects of Electromagnetic Fields*, (C. Polk, and E. Postow, eds.), CRC Press, Inc., Boca Raton, pp. 27.

Fricke, H., 1953, The Maxwell-Wagner dispersion in a suspension of ellipsoids, *J. Phys. Chem.*, **57**:934–937.

Gabriel, S., Lau, R. W., and Gabriel, C., 1996[a], The dielectric properties of tissue: II. Measurements in the frequency range 10Hz to 20GHz, *Phys Med Biol.*, **41**:2251–2269.

Gabriel, S., Lau, R. W., and Gabriel, C., 1996[b], The dielectric properties of biological tissues: III. Parametric models for the dielectric spectrum of tissues, *Phys. Med. Biol.*, **41**:2271–2293.

Geddes, L. A., and Baker, L. E., 1967, The specific resistance of biological material—A compendium of data for the biomedical engineer and physiologist, *Med. Biol. Eng.*, **5**:271–293.

Geddes, L. A., and Sadler, C., 1973, The specific resistance of blood at body temperature, *Med. Biol. Eng.*, **11**:336–339.

Gersing, E., 1998, Monitoring temperature induced changes in tissue during hyperthermia by impedance methods, Proc. of the X.ICEBI, Universitat Politecnica de Cataluya.

Gielen, F., 1983, Electrical conductivity and histological structure of skeletal muscle. PhD Thesis, University of Twente, the Netherlands.

Gielen, F. L. H., Wallinga-de Jonge, W., and Boon, K. L., 1984, Electrical conductivity of skeletal tissue: experimental results from different muscles in vivo, *Med. Biol. Eng. Comput.*, **22**:569–577.

Gonçalves, S., Munck, J. C. de, Heethaar, R. M., Lopes da Silva F. H., and Dijk, B. W. van, 2000, The application of electrical impedance tomography to reduce systematic errors in the EEG inverse problem—a simulation study, *Physiol. Meas.*, **21**:379–393.

Grandqvist, C. G., and Hunderi, O., 1978, Conductivity of inhomogeneous materials: effective medium theory with dipole-dipole interaction, *Phys. Rev. B*, **18**:1554–1561.

Hanai, T., 1960, Theory of the dielectric dispersion due to the interfacial polarization and its application to emulsions, *Kolloid-Z.*, **171**:23–31.

Harreveld, A. van, Crowell, J., Malhtotra S.A., 1965, A study of extracellular space in central nervous tissue by freeze-substitution, *J. Cell Biol.*, **25**:117–137.

Harreveld, A. van, and Ochs, S., 1956, Cerebral impedance charges after circulatory arrest, *Am. J. Physiol.*, **187**:203–207.

Hart, F. X., Berner N. J., and McMillen R. L., 1999, Modelling the anistropic electrical properties of skeletal muscle, *Phys. Med Biol.*, **44**:413–421.

Hashin, Z., and Shtrikman S., 1962, A variational approach to the theory of the effective magnetic permeability of multiphase materials, *J. Appl. Phys.*, **33**:3125–3131.

Havstad, J. W., 1967, Electrical impedance of cerebral cortex: an experimental and theoretical investigation, PhD Thesis, Stanford University.

Hoekema, R., Huiskamp, G. J. M., Wieneke, G. H., Leijten, F. S. S., van Veelen, C. W. M., van Rijen, P. C., and van Huffelen, A. C., 2001, Measurement of the conductivity of the skull, temporaily removed during epilepsy surgery, *Biomed Tech.*, **46**:103–105.

Homma, S., Musha, T., Nakajima, Y., Okamoto, Y., Blom, S., Flink, R., Hagbach, K. E., and Moström, U., 1994, Location of electric current sources in the human brain estimated by the dipole tracing method of the scalp-skull-brain (SSB) head model, *Electroen. Clin. Neuro.*, **91**:374–382.

Kobayashi, N., and Yonemura, K., 1967, The extracellular space in red and white muscles of the rat, *Jap. J. Physiol.*, **17**:698–707.

Kotnik, T., Bobanović, F., and Miklavčič, D., 1997, Sensitivity of transmembrane voltage induced by applied electric fields-a theoretical analysis, *Bioelectroch. Bioener.*, **43**:285–291.

Law, S. K., 1993, Thickness and resistivity variations over the upper surface of the human skull, *Brain Topogr.*, **6**:99–109.

Ludt, H., and Hermann, H. D., 1973, In vitro measurement of tissue impedance over a wide frequency range, *Biophys. J.*, **10**:337–345.

Maxwell, J. C., 1891, A treatise on electricity and magnetism, volume 1, Arts. 311–314, Dover Publ., New York.

Mc Rae, D. A., and Esrick, M. A., 1993, Changes in electrical impedance of skeletal muscle measured during hyperthermia, *Int. J. Hyperthermia*, **9**:247–261.

Nicholson, C., and Rice, M. E., 1986, The migration of substances in the neural microenvironment, *Ann. New York Academy of Sciences*, **481**:55–71.

Nicholson, P. W., 1965, Specific impedance of cerebral white matter, *Exp. Neurol.*, **13**:386–401.

Oostendorp, T. F., Delbeke, J., and Stegeman, D. F., 2000, The conductivity of the human skull; Results of in vivo and in vitro measurements, *IEEE T. Bio-Med. Eng.*, **47**:1487–1492.

Peters, M. J., Hendriks, M., and Stinstra, J. G., 2001, The passive DC conductivity of human tissue described by cells in solution, *Bioelectroch.*, **53**:155–160.

Pehtig, R., and Kell, D. B., 1987, The passive electrical properties of biological systems: their significance in physiology, biophysics and biotechnology, *Phys. Med. Biol.*, **32**:933–970.

Pfützner, H., 1984, Dielectric analysis of blood by means of a raster-electrode technique, *Med. Biol. Eng. Comput.*, **22**:142–146.

Plonsey, R., and Barr, R.C., 1986, Effect of microscopic and macroscopic discontinuities on the response of cardiac tissue to defibrilating (stimulating) currents, *Med. Biol. Eng. Comput.*, **24**:130–136.

Plonsey, R., and Heppner, D.B., 1967, Considerations of quasi-stationarity in electrophysiological systems, *Bulletin of mathematical Biophysics*, **29**:657–664.

Raicu, V., Saibara, T., and Irimajiri, A., 1998[a], Dielectric properties of rat liver in vivo: a non-invasive approach using an open-ended coaxial probe at audio/radio frequencies, *Bioelectroch. Bioener.*, **47**: 325–332.

Raicu, V., Saibara, T., Enzan H., and Irimajiri, A., 1998[b], Dielectric properties of rat liver in vivo: analysis by modeling hepatocytes in the tissue architecture, *Bioelectroch. Bioener.*, **47**:333–342.

Robillard, P. N., and Poussart Y., 1977, Specific-impedance measurements of brain tissues, *Med. Biol. Eng. Comput.*, **15**:438–445.

Rosell, J., Colominas, J., Riu, P., Pallas-Areny, R., and Webster, J. G., 1988, Skin impedance from 1 Hz to 1 MHz, *IEEE T. Bio-Med. Eng.*, **35**:649–651.

Rush, S., 1967, A principle for solving a class of anisotropic current flow problems and applications to electro-cardiography, *IEEE T. Bio-Med. Eng.*, **BME-14**:18–22.

Rush, S., Abildskov, J.A., and Mc Fee, R., 1963, Resistivity of body tissues at low frequencies, *Circ. Res.*, **XII**:40–50.

Rush, S., Mehtar, M., and Baldwin, A. F., 1984, Normalisation of body impedance data: a theoretical study, *Med. Biol. Eng. Comput.*, **22**:285–286.

Schwan, H. P., 1985, Dielectric properties of cells and tissues, in: *Interactions between Electromagnetic Fields and Cells,* (A Chiabrera, C. Nicolini, and H. P. Schwan, eds.) NATO ASI series, vol. 97, Plenum Press, New York, pp. 75–103.

Schwan, H. P., and Foster, K. R., 1980, RF-Field interactions with biological systems: Electrical properties and biophysical mechanisms, *Proc. of the IEEE*, **68**:104–113.

Schwan, H. P., and Takashima, S., 1993, Electrical conduction and dielectric behaviour in biological systems, *Encyclopedia of Applied Physics*, **5**:177–199.

Sekine, K., 2000, Application of boundary element method to calculation of the complex permittivity of suspensions of cells in shape of $D_{\infty h}$ symmetry, *Electroch.*, **52**:1–7.

Semrov, D., Karba, R., and Valencic, V., 1997, DC Electrical stimulation for chronic wound healing enhancement. Part 2. Parameter determination by numerical modelling, *Bioelectroch. Bioener.*, **43**:271–277.

Sillars, R. W., 1937, The properties of a dielectric containing semi-conducting particles of various shapes, *J. Ins. Electrical Eng.*, **80**:378–394.

Stanley, P. C., Pilkington, T. C., and Morrow, M. N., 1986, The effects of thoracic inhomogeneities on the relationship between epicardial and torso potentials. *IEEE T. Bio-Med. Eng.*, **BME-33**:273–284.

Stanley, P. C., Pilkington, T. C., Morrow, M. N., and Ideker, R. E., 1991, An assessment of variable thickness and fiber orientation of the skeletal muscle layer on electrocardiographic calculations, *IEEE T. Bio-Med. Eng.*, **38**:1069–1076.

Stinstra, J. G., 2001, Reliability of fetal magnetocardiography, PhD thesis, University of Twente, the Netherlands.

Stuchly, M. A., and Stuchly, S. S., 1980, Dielectric properties of biological substances-Tabulated, *J. Microwave Power*, **15**:19–26.

Takashima, S., 1989, *Electrical properties of biopolymers and membranes*, IOP Publishing Ltd, Bristol.

Trautman, E. D., and Newbower, R. S., 1983, A practical analysis of the electrical conductivity of blood, *IEEE T. Bio-Med. Eng.*, **BME-30**:141–153.

Ülgen, Y., and Sezdi, M., 1998, Electrical parameters of human blood, Proceedings 20th Ann. Int. Conference, IEEE/EMBS, Hongkong, 2983–2986.

Veelen, C. van, Debets, R., Huffelen, A. van, Emde Boas, W. van, Binnie, C., Storm van Leeuwen, W., Velis, D. N., and Dieren, A. van, 1990, Combined use of subdural and intracerebral electrodes in preoperative evaluation of epilepsy, *Neurosurgery*, **26**:93–101.

Yamamoto, T., and Yamamoto, Y., 1976, Electrical properties of epidermal stratum corneum, *Med. Biol. Eng.*, **3**:151–158.

Zheng, E., Shao, S., and Webster, J. G., 1984, Impedance of skeletal muscle from 1 Hz to 1 MHz, *IEEE T. Bio-Med. Eng.*, **BME-31**: 477–481.